Graduate School Form 30
Updated 1/15/2015

PURDUE UNIVERSITY
GRADUATE SCHOOL
Thesis/Dissertation Acceptance

This is to certify that the thesis/dissertation prepared

By Mahmoud Reza Zamani Farahani

Entitled

INTEGRATED MICRO PEM FUEL CELL WITH SELF-REGULATED HYDROGEN GENERATION FROM AMMONIA BORANE

For the degree of Master of Science in Mechanical Engineering

Is approved by the final examining committee:

Likun Zhu
Chair

Hazim Elmounayri

Mangi Agarwal

To the best of my knowledge and as understood by the student in the Thesis/Dissertation Agreement, Publication Delay, and Certification Disclaimer (Graduate School Form 32), this thesis/dissertation adheres to the provisions of Purdue University's "Policy of Integrity in Research" and the use of copyright material.

Approved by Major Professor(s): Likun Zhu

Approved by: Sohel Anwar 7/24/2015

Head of the Departmental Graduate Program Date

INTEGRATED MICRO PEM FUEL CELL WITH SELF-REGULATED HYDROGEN GENERATION FROM AMMONIA BORANE

A Thesis

Submitted to the Faculty

of

Purdue University

by

Mahmoud Reza Zamani Farahani

In Partial Fulfillment of the

Requirements for the Degree

of

Master of Science in Mechanical Engineering

August 2015

Purdue University

Indianapolis, Indiana

I dedicate this thesis to my family and specially my parents Alireza and Sorour who have been always supportive of my education and showed me the way of life. They are forever my role models in life.

ACKNOWLEDGMENTS

I would like to thank Dr. Likun Zhu for his endless academic and financial support during my research and study, and provisions above the academic contexts. I would like to thank my committee members for their assistance and supervision in preparation of this thesis. I would also like to thank our research group for being helpful with their tips during my research specially Cheolwoong Lim and Yuanzhi Cao. Finally, I reserve special thanks for my family, for their boundless mental, emotional, and financial support during my hard work. This research was made possible with the financial support of IUPUI RSFG and National Science Foundation under Grant No. 1264739.

TABLE OF CONTENTS

Page

LIST OF FIGURES

Figure Page

ABBREVIATIONS

AB	Ammonia Borane
GDL	Gas Diffusion Layer
HP	Hydrogen Peroxide
IPA	Isopropyl Alcohol
MEA	Membrane Electrode Assembly
PEM	Proton Exchange Membrane
PEMFC	Proton Exchange Membrane Fuel Cell
PS	PolyStyrene
SB	Sodium Borohydride
SS	Stainless Stell
WNS	Wood's Nickel Strike

ABSTRACT

Zamani Farahani, Mahmoud Reza. M.S.M.E., Purdue University, August 2015. Integrated Micro PEM Fuel Cell With Self-Regulated Hydrogen Generation From Ammonia Borane. Major Professor: Dr. Likun Zhu.

An integrated micro PEM fuel cell system with self-regulated hydrogen generation from ammonia borane is reported to power portable electronics. Hydrogen is generated via catalytic hydrolysis reaction of ammonia borane solution in microchannels with nanoporous platinum catalyst electroplated inside the microchannels. The self-regulation of the ammonia borane solution is achieved by using directional growth and selective venting of hydrogen bubbles in microchannels, which leads to agitation and addition of fresh solution without power consumption. The device is fabricated on combination of polystyrene sheets cut by graphic cutter, a stainless steel layer cut using wire electrical discharge machining and bonding layers with double-sided Polyimide tape. Due to the seamless bonding between the hydrogen generator and the micro fuel cell, the dead volume in the gas connection loops can be significantly reduced and the response time of self-regulation is reduced.

1. INTRODUCTION

1.1 Introduction

Fossil fuels have been vastly used as the main source of energy for many years. Over the past couple of years, there has been growing concern about the consequences of using such natural resources. Not only they will affect the environment by polluting the air and as a result causing the global warming but also the supplies for such energy resources are limited and due to latter. The cost of these energy resources will increase inevitably in the future and will have long term effects on the economy because many countries still depend on the foreign oil suppliers. As a result of these issues, for the past decade, there has been a growing interest in substituting fossil fuels with the alternative energy resources such as solar, wind, and water [1].

As the technology improves, the need for portable devices capable of storing and producing electrical energy increases. As a result of this demand, great deals of researches have been focused on providing renewable and environment-friendly electrochemical systems and micro power generators to provide the energy needed to run such devices. As cell phones and laptops get more functions and better performances, the need for better power resources to provide such power become vital. The current solutions for the micro power generators are power sources such as capacitors, batteries, fuel cells and biofuel cells. As you can see in the regime map in Figure 1.1, the power density and energy density for such power sources are represented. The capacitors have very high power density but their energy density is low. On the other hand, the biofuel cells have high energy density but their power density is low. Our target leans us toward two possible solutions: fuel cells and batteries. Fuel cells have higher energy density in comparison to batteries while batteries have slightly higher

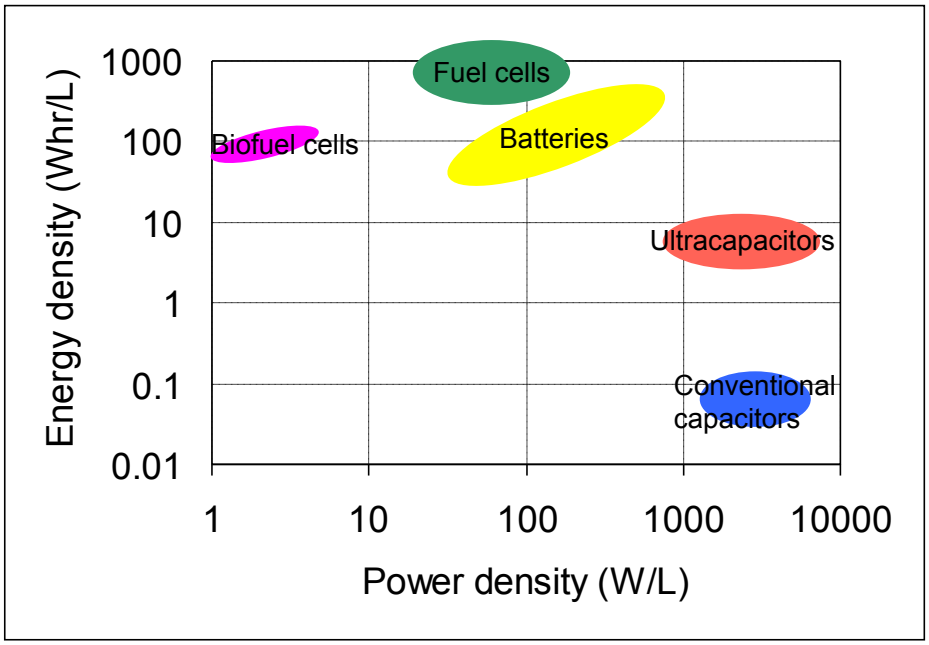

Figure 1.1. Modified Ragone plot of the domains for various power sources [2]

power density. We decided to focus our research on fuel cells due to their higher energy density, which is more important for portable electronics.

1.2 Fuel Cell Principles

Fuel cells convert chemical energy to electrical energy. The oxidation occurs at the anode where electrons are extracted and then travel through the external circuit resulting in electricity production. When they arrive at the cathode, they participate in the reduction reaction. The most common types of fuel cells are: Alkaline fuel cell (AFC), Phosphoric acid fuel cell (PAFC) and Proton Exchange Membrane fuel cell (PEMFC). Compared to the other types of fuel cells, Hydrogen PEMFCs show the potential for making micro power generators due to their low temperature operation, low weight and sustained operation at high current density, therefore are chosen to be studied in our research [3, 4].

Membrane Electrode Assembly (MEA)

The most important part of the cell is known as Membrane Electrode Assembly (MEA). A complete MEA is usually made of seven layers as you can see in Figure 1.2. Two layers of gasket (for sealing purposes), two layers of Gas Diffusion Layer (GDL), two layers of catalyst layer (one for the anode and one for the cathode side) and at the center Proton Exchange Membrane. [5] The Proton Exchange Membrane

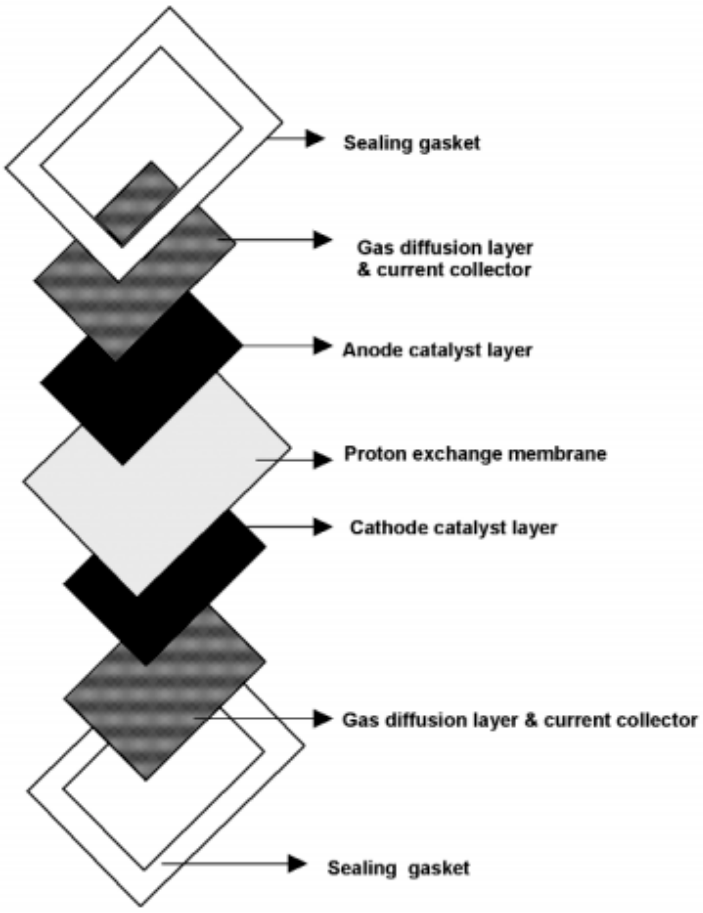

Figure 1.2. Schematics of a seven layer MEA [5]

is usually made of Nafion which has a Poly-tetrafluoroethylene (PTFE) backbone. The thinner the membrane, the lower the resistant for protons movements. But at the same time it will suffer from less mechanical strength and high fuel crossover. Therefore, nowadays usually membranes are made of composite polymers. The most

common nafion membranes' thickness varies anywhere between 25 to 100 μm [6]. The catalyst layer on the membrane is made of carbon supported metal catalyst. Carbon supported catalysts minimize the use of expensive metals. The most common metal used in the fuel cell industry is Platinum (Pt). The loading of Pt depends on the type of application and the fuel source which can vary anywhere from 80% Pt to 5% Pt. Since Pt is an expensive catalyst, many researchers today have focused on different methods to use less platinum in the catalyst layer and to create highly conductive carbon using mainly nanotechnology methods [7–9]. The catalyst layer are initially prepared as an ink and then are sprayed on Teflon decals. Later, the membrane is sandwiched between two teflon decals via hot press and as a result the catalyst layer is transferred to on the surface of the membrane [10].

The Gas Diffusion Lasyer is another important part of the MEA. The presence of GDL not only acts a protective layer for the thin catalyst layer but also uniformly distributes the gas source that come from the flow channels along the surface of the catalyst. It facilitates reactants' diffusion across the catalyst layer of MEA due to its surface area and porous structure. GDL also helps manage the fuel cell moisturte by helping with the removal of the byproducts that may cause flooding the chambers. GDL is usually made of carbon paper which makes it hydrophobic specially fir moisture control. The hydrophobicity of the GDL is important especially on the cathode side where water should be easily repelled from the catalyst surface [11].

1.2.1 Hydrogen Proton Exchange Membrane Fuel Cells

PEM fuel cells are promising candidates for micro power generation as mentioned in the previous section. The structure of a PEM fuel cell is very simple as you can see in Figure 1.3. Hydrogen is oxidized in anode and oxygen is reduced in cathode. When the hydrogen is delivered to the anode, the anode catalyst will break the hydrogen to protons and electrons. The protons diffuse to the cathode through the membrane, and electrons travels along an external circuit to the cathode. So it can generate power.

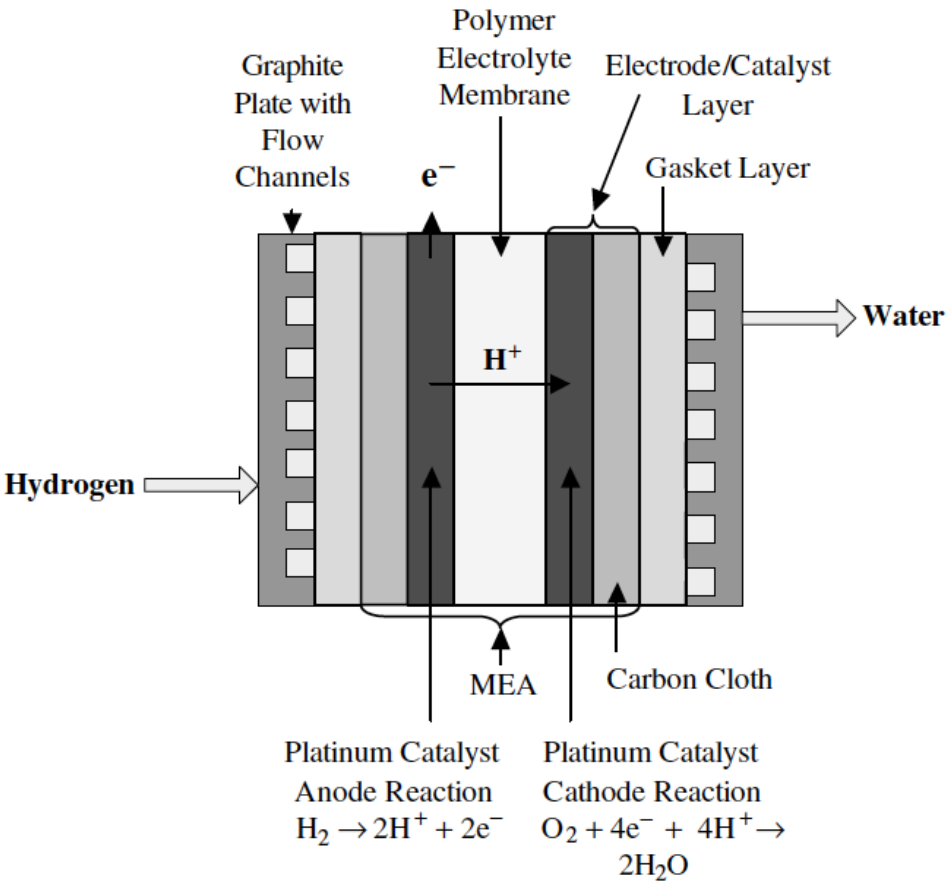

Figure 1.3. Schematics of a hydrogen PEM fuel cell [12]

The protons, electrons and oxygen will react at the cathode catalyst to generate water [12].The typical reaction formulas are listed below:

$$Anode : \mathrm{H_2} \longrightarrow 2\,\mathrm{H^+} + 2\,\mathrm{e^-}$$

$$Cathode : \mathrm{O_2} + 4\,\mathrm{e^-} + 4\,\mathrm{H^+} \longrightarrow 2\,\mathrm{H_2O}$$

$$Overall : \mathrm{H_2} + \frac{1}{2}\mathrm{O_2} \longrightarrow \mathrm{H_2O} + \mathrm{Electricity} + \mathrm{Heat}$$

The theoretical open circuit voltage for a cell reaction is 1.23 V. Figure 1.4 shows a typical polarization curve for a hydrogen fuel cell. As you can see the curve is divided into three main regions: kinetics limited region, ohmic region and mass transport limited region. In the first region, fuel cell has lower power demand and high voltage with lower value of current density. These loses are associated with the kinetics of the

electrodes and specifically slow rate of oxygen reduction at the cathode. The losses in the second region (ohmic region) are caused by resistance between electrolyte and electrodes or generally internal component of the fuel cell. The final region (mass transport limited) occurs at low voltage and high current density due to fast rate of electrochemical reactions at the electrodes to meet the power demand. Current density reaches a limiting value where mass transfer of reactants limits the reaction [13, 14].

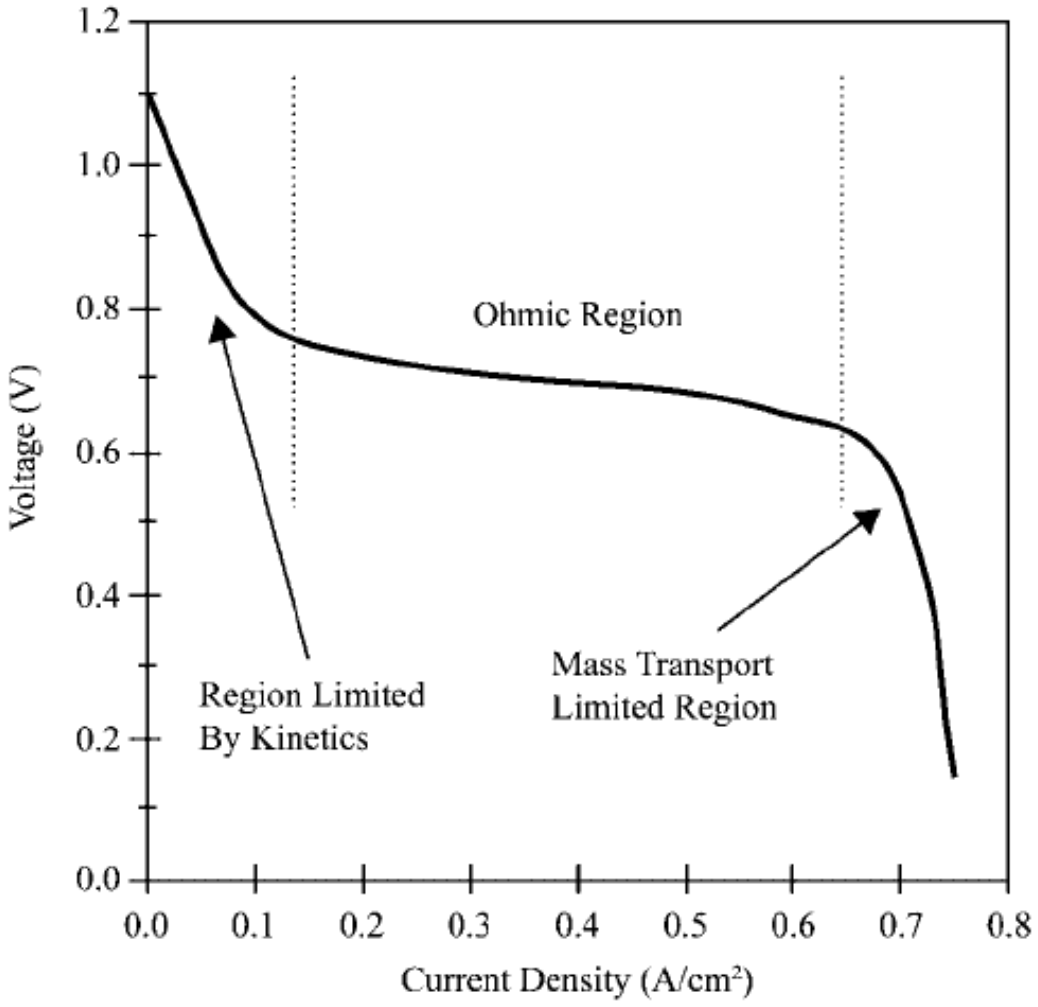

Figure 1.4. A typical hydrogen fuel cell polarization curve [15]

1.2.2 Micro Hydrogen Fuel Cells

Micro fuel cells are the main candidates for the next generation of portable electronics like personal digital assistant, laptops, cell phones and such. As batteries go through a chemical process to create energy, micro fuel cells are able to provide longer portable power but pure hydrogen feeding of a micro fuel cell in electronic devices can be difficult due to problems associated with storage of hydrogen gas in such small size. Micro hydrogen fuel cells can be divided into two main categories: "micro hydrogen fuel cell system" which include the micro fuel cell and an onboard hydrogen supplying system and "hydrogen fed micro fuel cells" in which the micro fuel cell and the hydrogen supplying mechanism are separated. We will be mainly focused on the micro fuel cell systems since that is the goal of this project.

Micro Hydrogen Fuel Cell System

These kinds of micro fuel cells can operate in both high and low temperature depending on the type of fuel they are fed. Usually methanol is used at high temperature applications and sodium borohydride in the lower temperature. But as we discussed in the previous sections, sodium borohydride has given its place to ammonia borane. To this day, most of the micro hydrogen fuel cells are fabricated based on micro electromechanical system or MEMS [16–18]. The main issue with Si wafer based micro fuel cell is its fragility which will prevent compressing the fuel cell tightly for better sealing [19]. Our design as we will discuss in the next chapter is not fragile and is made of a combination of stainless steel and polystyrene which will address this issue.

Hydrogen generation from hydrides through using metallic catalysts is an attractive subject because it is an easy and feasible technology though the main setback is the presence of byproducts. To address this issue previously researchers have tried to use lower concentration of hydrides in the range of 10% to 15% [20–22]. But all those efforts are focused on using sodium borohydride which show there is a much

needed study on ammonia borane specifically in micro scale. There has been only one literature using ammonia borane in micro hydrogen generation system but the system and the micro fuel cell are not integrated and the generated hydrogen is fed through tubes to the micro fuel cell [23].

1.3 Hydrides for Micro Scale Hydrogen Generation

As we discussed a PEM fuel cell's principles in the previous section, the importance of hydrogen as the fuel to power the cell has become obvious. Assume the fuel cell is operating at 0.6 V with hydrogen at 1 atm and room temperature. The gravimetric energy density of hydrogen is 16000 Whr/kg, but the volumetric energy density is 1.3 Whr/L [24]. At micro scale, in most of the cases, volumetric density is more important. So it causes two challenges in our work. The first one is high volumetric energy density hydrogen storage materials and the second one is how to control the hydrogen generation onboard. In this section we will address the first challenge and the second challenge will be addressed in the next section. Hydrogen can be stored in different forms, such as gas, liquid, reforming certain chemicals [25, 26] and metal or chemical hydrides [27–29]. Unfortunately many of them are not suitable in micro scale hydrogen generation because of low energy density. The regime map in Figure 1.5 shows the hydrogen mass density and volume density of some hydrogen storage materials. The compressed hydrogen and the liquid hydrogen are here. They have 100 percent mass density, but the volume density is low. There are some hydrocarbon fuels with high energy densities, but they need to be reformed at high temperature to generate hydrogen. We need materials with both high mass density and volume density. From the figure we can observe that most of hydrides fall in this category and they can generate hydrogen with easy reactions.

Nowadays, a lot of researches are being conducted on hydrogen generation via hydrolysis of chemical and metal hydrides especially for hydrogen PEM fuel cells.

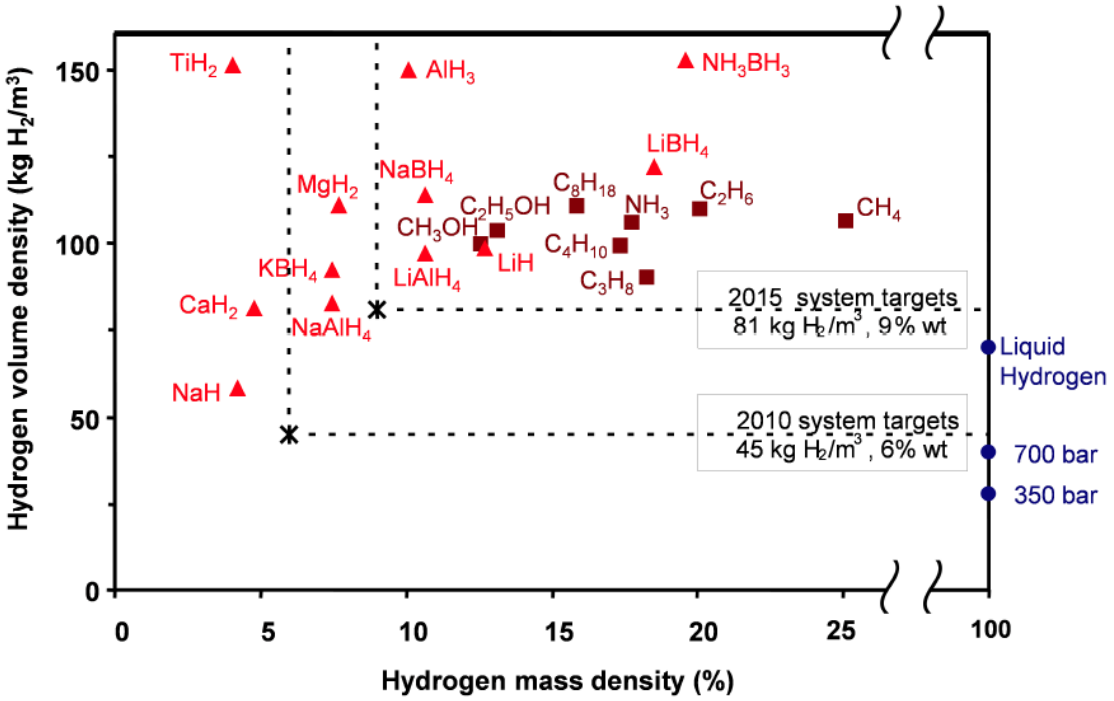

Figure 1.5. A regime map of hydrogen densities for different materials containing hydrogen and U.S. Department of Energy's targets for 2010 and 2015 [29]

Among these materials, Sodium Borohydride ($NaBH_4$; SB) has been extensively studied [29–32].

In presence of a proper catalyst, SB reacts rapidly with water to produce hydrogen:

$$NaBH_4 + 2\,H_2O \xrightarrow{\text{Catalyst}} NaBO_2 + 4\,H_2 \tag{1.1}$$

The other chemical that recently has attracted a lot of attraction is Ammonia Borane (AB), which is very similar to sodium borohydride when it comes to properties. The room temperature catalytic hydrolysis of AB is:

$$NH_3BH_3 + 2\,H_2O \xrightarrow{\text{Catalyst}} NH_4^+ + BO_2^- + 4\,H_2 \tag{1.2}$$

In the next section we will compare these two materials and justify our choice of ammonia borane for our research.

1.3.1 Ammonia Borane vs Sodium Borohydride

	AB	SB
Properties	NH_3BH_3	$NaBH_4$
Molecular formula	30.7	37.8
Hydrogen Storage Capacity (wt%)	19.5	10.8
Hydrogen Storage Capacity ($g(H_2)/L$)	152	133
Safety		
Stability	Moisture Sensitive	Moisture Sensitive
Stability of Aqueous Solution	High Stability	Self-Hydrolysis (stabilized with addition of NaOH)

Figure 1.6. A side by side comparison of AB and SB properties and safety [33]

Ammonia borane has most recently stepped into the spotlight ever since the U.S. Department of Energy announced a no-go for further study and development of SB in automobile applications [33].You can see a side by side comparison of AB and SB in Figure 1.6. AB with 19.6wt% has a higher gravimetric hydrogen content than SB with only 10.8 wt.%, unlike SB, is very stable in neutral water (PH = 7) and does not demand addition of NaOH to elevate the pH and stabilize the solution. It has been also shown that other significant advantages of AB over SB such as higher hydrogen generation rate for AB in comparison with SB and better durability of catalyst [23].The last two are especially important to us for our research since we are looking for better Hydrogen generation to feed the fuel cell and also make our device as durable as possible. You can see the hydrogen generation profile of both materials in Figure 1.7. As you can see while AB experience a 15% degradation SB is degraded 50% in the same amount of time.

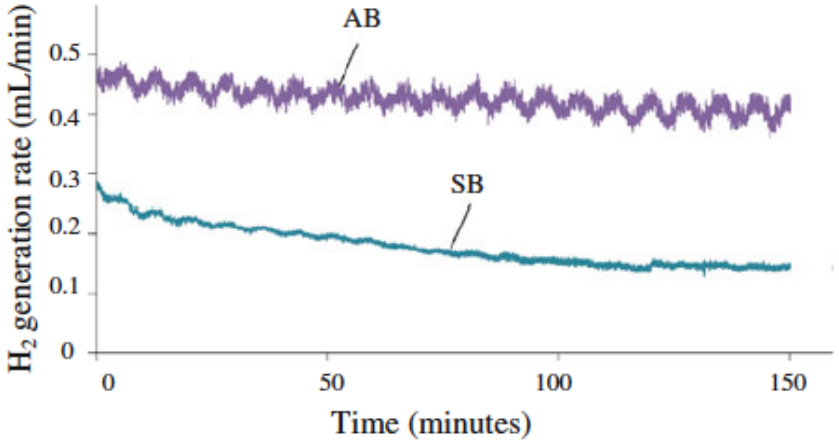

Figure 1.7. Hydrogen generation rate 1% solutions of AB and SB [23]

1.3.2 Ammonia Borane Dehydrogenation

There are two main methods for ammonia borane dehydrogenation : thermolysis and catalyst hydrolysis [34–36]. There are problems associated with thermolysis when it comes to fuel cell applications although hydrolysis produces lower theoretical hydrogen. Thermolysis requires relatively high temperatures (at 150^{o}C) to release 2 equivalent of hydrogen per AB and if we want the final molar equivalent hydrogen we need to raise the temperature to around 450^{o}C. The present day fuel cells operate at lower temperatures (around 80^o C). At this temperature the hydrogen generation time using thermolysis is about 200 minutes [37]. Therefore for micro fuel cell application the hydrolysis of ammonia borane using catalysts is favored.

Many reseraches have been focused on ammonia borane dehydrogenation using transition metals specially Platinum group metals like Platinum, Palladium and Ruthenium [38–40]. According to both Chandra et al. [38] and shrestha et al. [40] platinum catalyst has the highest catalytic activity as you can see in Figure 1.8.

We already know when it comes to use platinum as the catalyst we have a choice of differnt variation of Pt catalys specially carbon supported platinum. But among these variations the catalytic activity of 20 wt. % Pt/C is the highest as can be

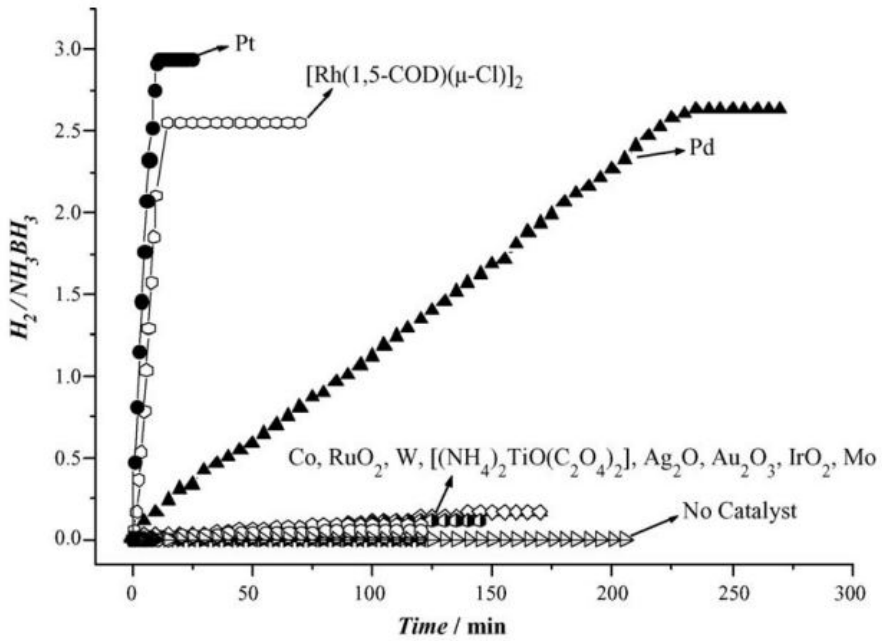

Figure 1.8. Hydrogen generation from 0.33 wt.% aqueous ammonia borane [38]

seen in Figure 1.9. But one of the rquirements of our device is the hydrphilicty of the reaction channels and in turn hydrophilicty of the catalyst layer. Eventhough carbon supporetd platinum variations show better catalytic activity but the presence of carbon in the structure will make the catalyst layer hydrophobic and not useful for our application. Therefore, in our research we decided to use Pt black as our catalyst.

1.4 Onboard Micro Hydrogen Generation

Many reasearches have been focused on using a hydride based micro hydrogen generator to fulfill the need for power in micro fuel cells. Moghaddam et al. [41] created a self-regulating hydrogen generator free of need for external power to operate. Hydrogen was generated by reaction of metal hydrides with water vapor. The device consists of two chambers on top of each other. The top chamber is filled with water with single port into the lower chamber and is separated from the hydride chamber

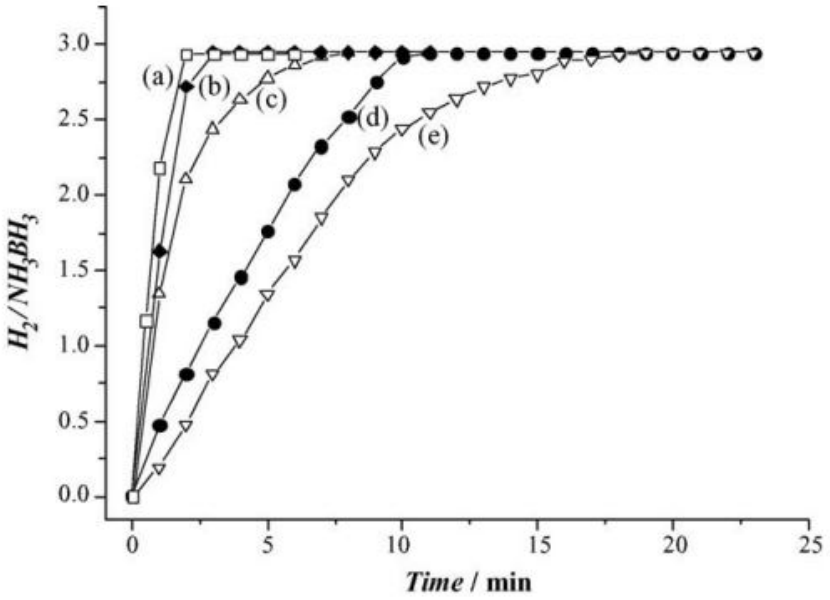

Figure 1.9. Hydrogen generation profle of 0.33 wt.% aqueous ammonia borane for (a) 20 % Pt/C (b)40 % Pt/C (c) PtO_2 (d) Pt black (e) K_2PtCl_4 [38]

below it with a polyimide membrane with two holes in it. The self-regulating mechanism works based on the gas pressure inside the hydride chamber and the membrane deflection. The integrated air-breathing micro fuel cell was able to produce nearly 8 ma/cm^2 at 0.3 V.

Swaminathan et al. [42] fabricated a 4.4 mL capacity microfluidic based self-regulating onboard hydrogen generator that uses hydrides (CaH_2 and LiH_4) and water reaction to generate hydrogen. The device consists of two side by side chambers: one for water and one for the hydride. There are holes aligned with chambers and are connected by a hydrophilic channel. Channel is then fully fabricated using a polyimide diaphragm which is bonded to the bottom of the control layer. The device relies on passive surface based pumping mechanism. When power is needed by the micro fuel cell, water will flow in the channel and vapor will be diffused through a hydrophobic membrane in order to react with the hydride. When electrical load is cut

off, hydrogen accumulates between MEA and diaphragm causing a pressure difference that will eventually close the water chamber outlet.

Taegyu Kim [22] build a hydrogen generator based on chemical hydride ($NaBH_4$) reaction with cobalt-phosphorous-boride catalyst layer. They used a micro pump with external power (battery) to pump $NaBH_4$ inside the catalyst channel. Hydrogen diffuses through a porous membrane that separates the channel from the hydrogen container while NaBO2 solution returns to the fuel cartridge.

Zhu et al. [23] designed a self-regulated and self-circulated microfluidic hydrogen generator that generates hydrogen by self-pumping ammonia borane (NH_3BH_3) solution into catalyst channels filled with platinum black. The hydrogen outlet of the device was then connected to a fuel cell via tube. This research is what this manuscript is built on.

As you can see from the literature review, majority of research in onboard hydrogen generators and integrated fuel cell systems in micro scale is focused on using metal hydrides or chemical hydrides. (NH_3BH_3) has higher hydrogen volume density and mass density compared to metal hydrides and is stable in D.I. water at room temperature. Other advantages of ammonia borane is discusses in details in the previous section.

1.5 Objective of This Thesis

In this thesis, we used ammonia borane solution in D.I. water due to its advantages not only over metal hydrides but also over ($NaBH_4$) as discussed in the previous sections. Our device does not need an external powered pumping mechanism and is self-regulated. The advantage it has over the previous device made by Zhu and Meng is that there is no need to use a tube to feed hydrogen to the anode of the fuel cell since using tubes and connection may result is performance loss or even hydrogen leakage and it also will not make a compact design. Instead of using MEMS method and silicon based materials, we used a very inexpensive method of creating

our hydrogen generator using polystyrene film and a graphic cutter to form our layers and bonded them together with a polyimide double-sided tape. There are not as many researches conducted in ammonia borane base hydrogen generators as there are for sodium borohydride integrated micro hydrogen generators. Our goal is to design and fabricate an aqueous ammonia borane based self-pumping and slef-regulating hydrogen generator and directly integrate it with a fuel cell without using external connections.

2. THEORY

2.1 Operation Mechanism

In order to have the best possible microfluidic based hydrogen generator, our device should have passive micro-pump, passive micro-valve and gas-liquid separator. In other words, the device should be self-regulating to be able to control hydrogen generation based on the load (current demand in the fuel cell case) and also should be self-circulating to have less parasitic power consumption.

2.1.1 Self-circulation Mechanism

The self- circulation in this research is provided by a micro-pumping mechanism which is based on liquid and gas bubble directional growth plus a selective gas venting mechanism which has been previously reported by Meng and Kim. [43] This pumping mechanism has been further modified and further developed to adapt to our system that generates hydrogen from the reaction between our solution and catalyst. We chose Platinum-black as our catalyst and as mentioned before our solution is Ammonia Borane in water. In order to achieve the directional growth and also selective gas venting we need to pay attention to the surface properties inside our micro channels. Generally water tend to fill out flat, hydrophilic micro channels as a result of capillary pressure effect. As you see in Figure 2.1.a the directional growth and as a result creation of a virtual check valve can be achieved by creating a channel neck at the point where the cross section area of our micro channels suddenly changes. [43, 44] This channel neck causes a height difference inside the channel and as a result the bubbles will grow rightward inside the channels:

$$\Delta P_i^{max} = 2\delta(\frac{1}{h_i} + \frac{1}{w_i})cos\theta \tag{2.1}$$

As you can see from the formula, the maximum capillary pressure depends solely on the surface properties where δ is the liquid-gas interface surface tension, θ is the contact angle of liquid on the surface of the channel, h_i and w_i represents channel height and width (where i = 1,2). Since all the parameters except for the channel height is same on the both sides of the channel neck, it is obvious thatΔP_1^{max} is greater thanΔP_2^{max}. This pressure difference causes the bubble to grow rightward and as the next bubble gets to the channel neck the same thing will happen and eventually the bubbles keep pushing each other to the right side. The next challenge is to find

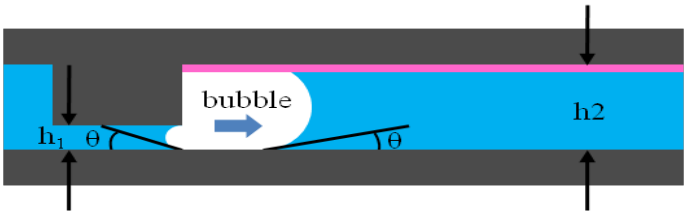

(a) Channel neck prevents the bubble to move to the left

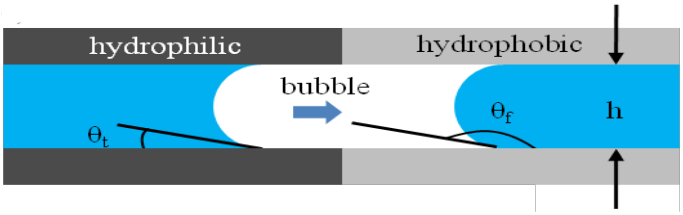

(b) A hydrophilic-hydrophobic junction to trap the bubble for better ventilation

Figure 2.1. Cross section view of the channels [43]

an efficient design to vent as much gas as possible. To address this issue again we will go back to the surface properties. The problem can be solved by introducing a hydrophilic-hydrophobic junction like the one you can see in Figure 2.1.b, where θ_f is the angle of the right minuscus and hydrophobic surface of the channel wall which applies a capillary pressure to move the bubble to the right side. The angle between the left meniscus and the hydrophilic surface inside the micro channel is represented by θ_t and is smaller than 90^o, which will apply a capillary pressure to move the bubble

to the right side as well. The total rightward capillary pressure applied upon the gas bubble is :

$$\Delta P_j = -2\delta(\frac{1}{h} + \frac{1}{w})(cos\theta_f - cos\theta_t) \tag{2.2}$$

where δ is the surface tension of liquid-gas interface, h represents the channel height, and w represents the channel width.The channel neck and the junction will work simultaneously to ensure the bubbles growth to the right side and the latter will also help with the better gas ventilation.

2.1.2 Self-regulation Mechanism

The process of hydrogen generation is regulated by the amount of reactant solution (in our case AB solution) allowed inside or forced out of the channels. In other words, when more hydrogen in consumed on the anode side of the fuel cell when extra load is applied, the AB solution will be circulated inside the channels with the maximum pumping rate to produce enough hydrogen bubbles in order to be able to feed the need of the fuel cell. The regulation is achieved because as the amount of hydrogen is increased, the contact area between the solution and catalyst will decrease and will cause less gas generation. On the other hand, when external load is removed from the fuel cell and hydrogen is not being consumed at the anode, the channels will eventually be filled with hydrogen gas and AB solution is forced out of the channels to stop the reaction and as a result stop further hydrogen generation.

The circulation can also adapt to the hydrogen consumption rate, meaning that the flow rate of the solution (pumping rate) can be regulated by the hydrogen consumption at the gas outlet. The more hydrogen is needed, the more the pumping rate of the solution. When gas is extracted at a rate less than the generation capability, pressure will increase and eventually result in lower gas removal rate and pumping rate until the system reaches equilibrium.

In our research, we will test this mechanism by using two different materials with 2 different concentrations:

1. 2% and 4% ammonia borane in D.I. water.

2. 4% and 8% hydrogen peroxide (H_2O_2) in D.I. water.

As we will discuss in more details in the third chapter, the self-regulation was achieved in both cases. The only difference is that the product of AB solution and Pt catalyst will be hydrogen while in the H_2O_2 case the gas generated is oxygen.

2.2 Integrated Microfluidic Hydrogen Generator

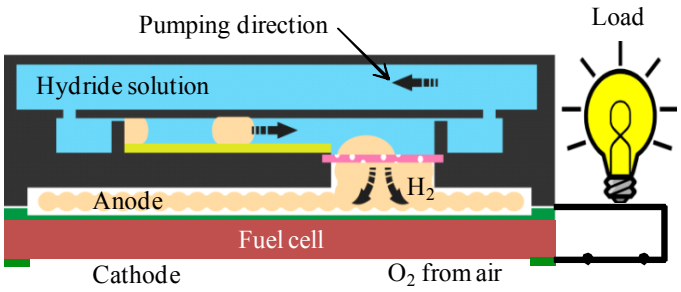

(a) External current is drawn

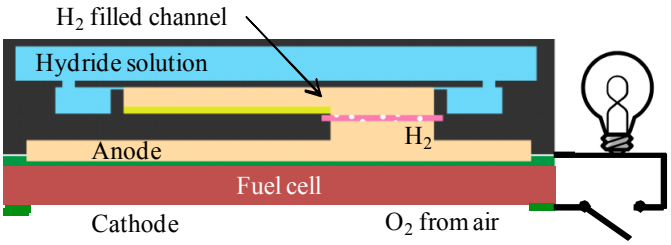

(b) External current is interrupted

Figure 2.2. Schematic of the fully-enclosed micro fuel cell and generator assembly

The proposed microfluidic hydrogen generator can provide a solution to solve the problem and facilitate the development and commercialization of micro fuel cells. The long term industrial outreach of this micro fuel cell study is to develop a low cost and high energy density portable hydrogen fuel cell which can replace current rechargeable batteries for portable electronics. To demonstrate the feasibility of a self-

regulating micro fuel cell system, the fabricated hydrogen generator will be integrated with a commercial hydrogen PEM fuel cell and the fuel cell performance will be investigated using an electrochemical analyzer. This fuel cell will use high energy density hydride fuel (NH_3BH_3) and charging the fuel cell can be simply achieved by replacing the hydride fuel cartridge. The full assembly, consisting of a hydrogen generator and a micro fuel cell, is schematically shown in Figure 2.2.The gas outlet of the hydrogen generator will be directly connected the anode inlet of the fuel cell and the cathode will be air breathing. The hydrogen pressure at the anode of the PEM fuel cell is employed to regulate the hydrogen generation rate. Hydrogen consumption within the fuel cell will initiate the self-circulation of liquid reactants within the generators. Reactions in the generators continue as long as hydrogen is consumed. However, once the circuit is opened, the gas generators will be stopped automatically to conserve the liquid fuel until its next usage. By eliminating the need for active pumps, valves, and gas-liquid separators, a micro power generator with higher energy density than rechargeable batteries can be developed. This integrated system also provides a platform to investigate the integration capability and limitation of the microfluidic reactor with a fuel cell.

3. FABRICATION

Our device consists of two main parts: onboard hydrogen generator and fuel cell. In this chapter we will explain the fabrication process for both parts.

3.1 Overview of Material Selection

As we previously discussed in Chapter 2, the principles we were looking for to make our hydrogen generator depend on the surface characteristics of the material we use, specially the materials that will form the channels. After examining different materials, we decided to make the hydrogen generator mainly from two materials: Polystyrene and stainless steel. The reasons behind our selection and how the surface characteristics we were looking for applied to these two materials will be discussed in the following sections.

3.1.1 Polystyrene

Polymers have been the focus of study in the biomedical field and microfluidics for a while. Microfluidic has made the study of cellular phenomena and modeling them much easier. [45–47] Among the polymers, polystyrene has attracted a lot attention for research in the cellular research. Polystyrene films are transparent, rigid and the surface characteristics can be easily modified by introducing functional groups. Polystyrene is not considered hydrophilic, but can be easily made hydrophilic by different chemical and physical methods. A common method of turning polystyrene hydrophilic is functionalizing the surface with plasma treatment.

3.1.2 Oxygen Plasma Treatment

Oxygen plasma treatment is one of most widely used methods to functionalize the surface of polymers and as a result making a hydrophilic surface. [48–51]By evacuating the reaction chamber, glow discharge plasma is formed. Electrons with high energy will hit the surface of polymer which is made of Carbon and Hydrogen (C-H) chains. This will result in combination of the oxygen radicals with the polymer chains. Consequently, functional groups of hydroxyl (-OH) or Carbonyl (C=O) are formed and will make the surface hydrophilic. Schematics of the process can be observed in Figure 3.1.

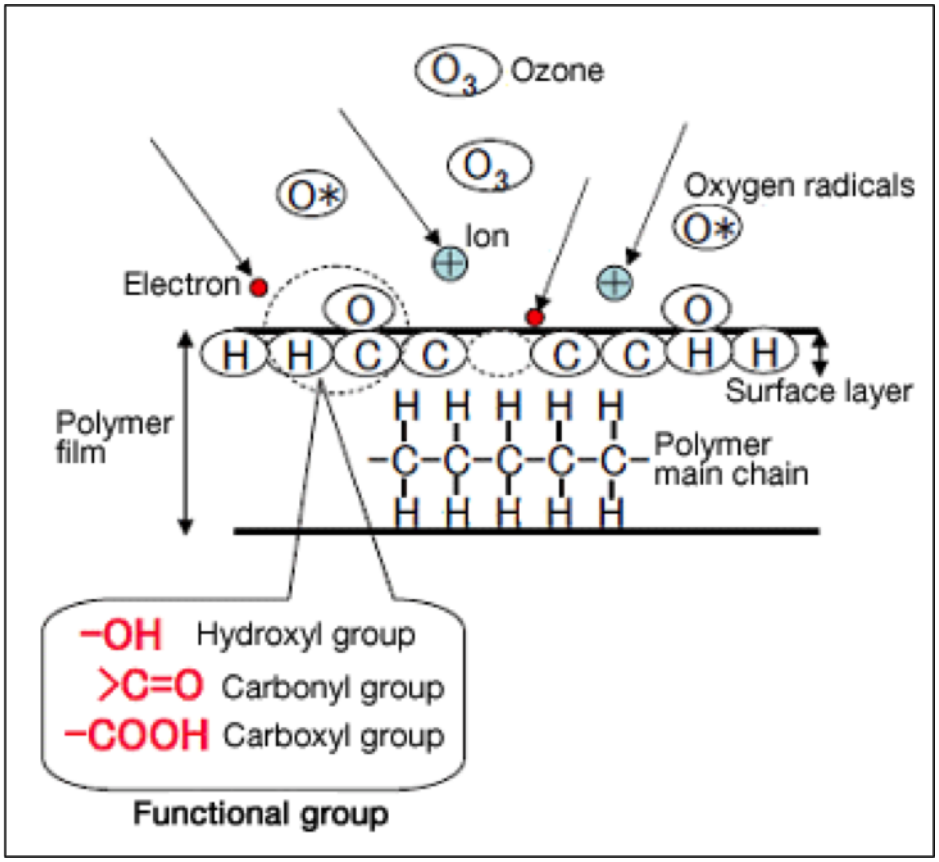

Figure 3.1. Schematics of a polymer oxygen plasma treatment [52]

3.1.3 Platinum Deposition

In order to deposit Platinum black inside the channels, we chose stainless steel as our substrate due to the conductivity and ease of Pt deposition. Then Pt was electroplated on the surface of stainless steel layer. But before electroplating Pt black, we need to prepare the stainless steel layer and improve the adhesion of Pt black to the surface. One of the most common methods to increase the quality and adhesion of Pt black to a stainless steel surface is Wood's Nickel Strike. Basically, in this process, a thin layer of Nickel is deposited on the surface of the stainless steel layer and the Pt black will be electroplated on the nickel to improve Pt black durability and adhesion to the surface. A computer model of the hydrogen generator is shown in Figure 3.2.

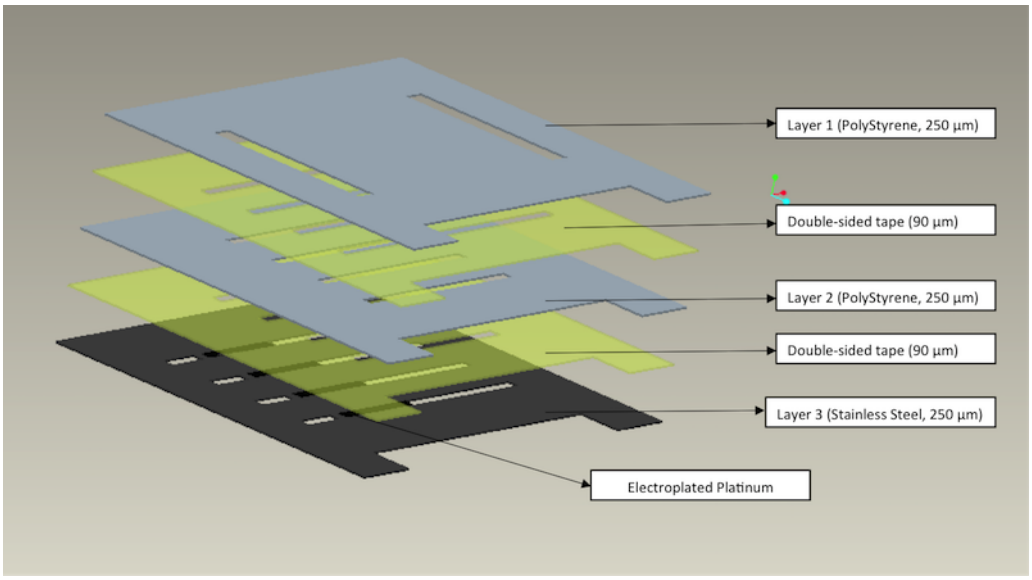

Figure 3.2. A layer by layer computer model of hydrogen generator

3.2 Hydrogen Generator Fabrication Process

In previous PS-based studies laser is mainly used to create and cut fine features in PS based microfluidic devices [53, 54]. Interactions between the laser light and the

polymer can induce unwanted surface modifications and also using laser will increase the overall cost of the project. Using digital desktop cutters is a low-cost and straight forward rapid prototyping method [55, 56]. In our study, we used Polystyrene films of 125 μm (Goofellow Corporation, Coraopolis, PA). We cut the Polystyrene film with Graphtec Cutter (Graphtec FC2250-60 VC) to form the first two layers of the hydrogen generator as shown in Figure 3.3. Layer 1 consists of two rectangular openings (20 x 2mm) that will be used as inlet and outlet for the solution. Layer 2, is the layers that forms the channels. Four channels of the same size (9 x 1mm) were cut using the cutter. Before bonding the layers together, we have to ensure that

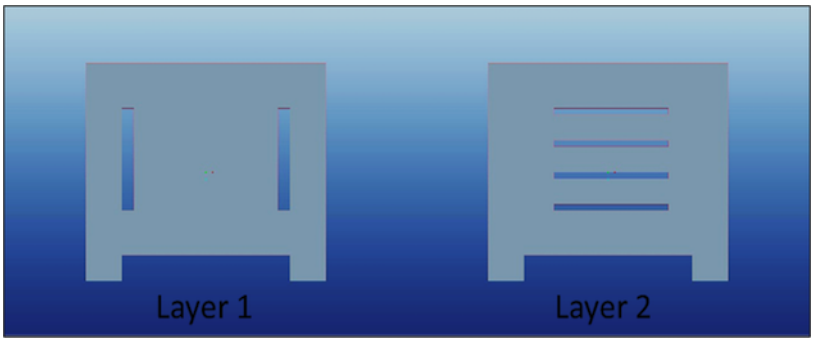

Figure 3.3. Schematics of the first two layers (polystyrene)

the surface in contact with the solution is hydrophilic. In order to achieve that, we will use oxygen plasma treatment to change the surface properties of polystyrene. Before the treatment the surface of PS film was cleaned by emerging in Isopropyl Alcohol (IPA) for 5 minutes and then the same for Ethanol. Then, the films were rinsed by D.I. water and were dried at room temperature. Treatment was performed using Plasma Etch PE-50XL. Although studies have shown the aging effect on the polymers after oxygen plasma treatment, meaning that the wettability properties decrease with time. The aging effect is caused by the surface rearrangement due to the extra interfacial free energy and mobility of polymer chains. [57,58] This problem can be solved if higher intensity oxygen plasma is performed (with self-bias voltage more than 140V) and increasing the treatment time. [59] In our study, total treatment

time was 6 minute with 2-minute intervals as you can see in Figure 3.4. Measurements of contact angle were done with Rame-Hart goniometer (Model 290). The untreated Polystyrene has a contact angle of close to 80^o which is not suitable for our application since the device depends on the hydrophilicity of the channel to be able to produce the sufficient capillary pressure. After 6 minutes of treatment the contact angle drops to just below 10^o and therefore matches our need for the channels' specification. After treatment, the layers were bonded together using double-sided Polyimide tape (Kaptontape, KPPTDE-2). By using transparent polystyrene layers and double-sided tape for bonding, we are also making the study easier since we are able to see the whole process of hydrogen generation and venting as it happens and therefore diagnose the potential problems the device may face.

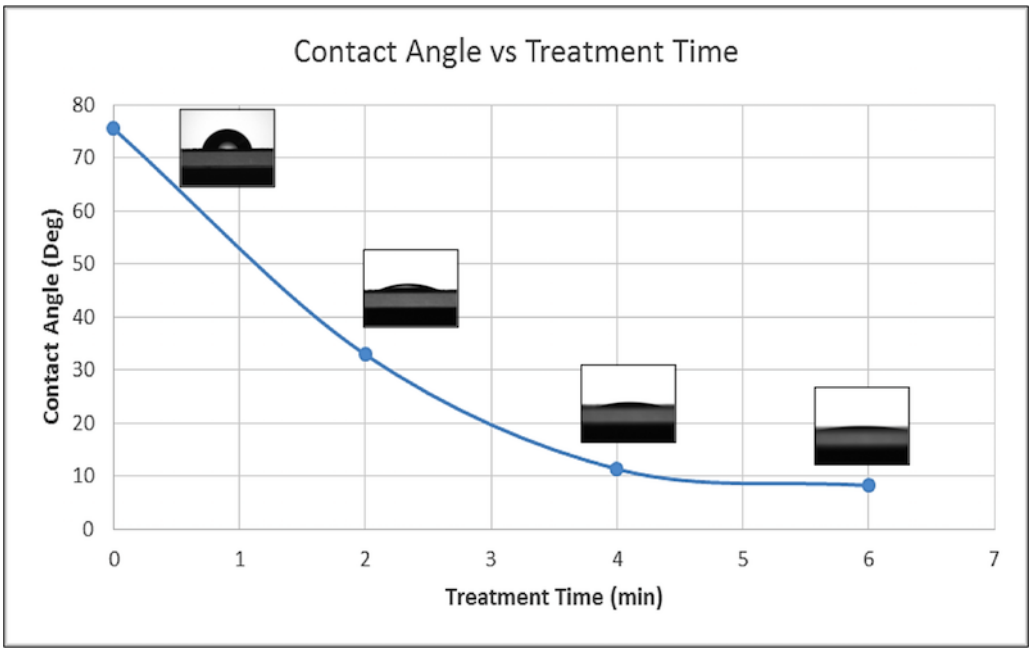

Figure 3.4. Contact angle of PS after 6 Minutes of treatment

3.2.1 Catalyst Deposition (Electroplating Pt Black)

As the first two layers are prepared and will form the inlet, out let and top surface of the channels, it is time to complete the hydrogen generator assembly by adding the catalyst which is deposited inside the channels in order to spark the hydrogen generation process. The substrate had to be cut very precisely therefore we used Wire Electro Discharge Machining (WEDM) process to achieve the maximum precision. Electric Discharge Machining (EDM) is one of the non-traditional machining processes. EDM is the process of machining electrically conductive materials by using controlled spark that is created between an electrode and a work-piece in the presence of a dielectric fluid [60]. EDM is a thermal process; material is removed by heat created as a result of the voltage difference between the electrically conductive work-piece and electrode. This process is divided in two main types: Die-sinking and Wire-EDM. The principle for both types is almost similar. Die-sinking needs the electrode to be machined in opposite shape as the one needed for the substrate. While WEDM uses a wire as electrode and a series of sparks happen from the side surface of wire to the substrate surrounded by dielectric fluid (usually D.I. water). The temperature in this method is between 8000 ^{o}C and 12000 ^{o}C [61, 62]. There are other differences between the two methods such as dielectric fluid, sparking and sparking area that can be studied but our main focus in this work is on WEDM. A basic WEDM machine is illustrated in Figure 3.5. Normally, a pin guide at the upper and lower parts of the work piece holds the wire. In most cases the wire, once used, will be discarded since the removed material from surface of the wire during the process will decrease the wire's strength [63].

The deposition method we selected is electroplating. Electroplating is most commonly used for corrosion prevention and decorating in every day life. In electroplating we use electric current to deposit a metal coating on to a certain area or object. The set up for electroplating is very similar to a galvanic cell. The substrate to be plated will be cathode, we need electroplating bath (electrolytic solution) and the anode

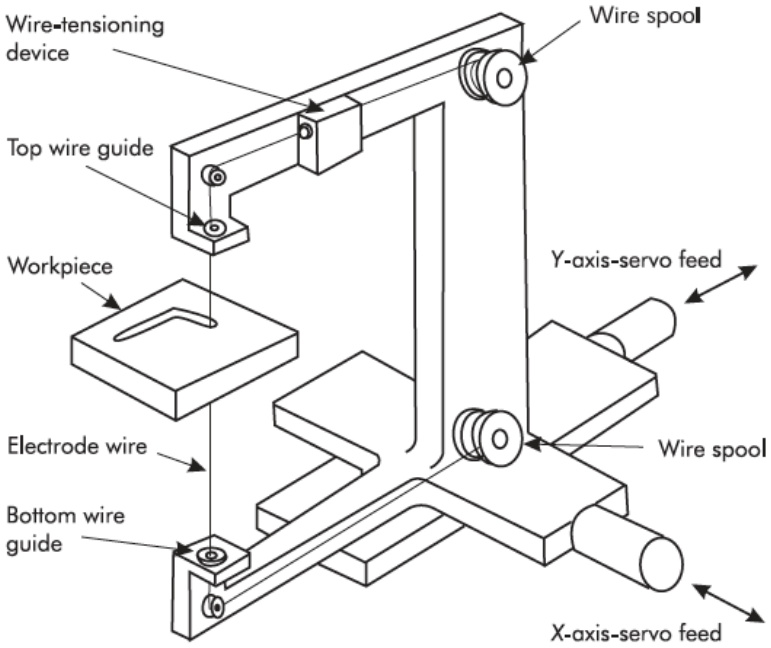

Figure 3.5. A basic WEDM machine illustration [60]

will be the metal we like to use for coating (in our case platinum). When external current is applied, platinum ions will migrate to cathode where they are reduced and deposited on the surface of stainless steel. In our study, we used a conventional three-electrode cell system. But as we mentioned earlier before further discussing the Pt black electrodeposition, we need to make sure that Pt black will be stable on the surface of stainless steel. In order to do so, we will first have to make sure the stainless steel is cleaned properly and second, since the substrate is stainless steel we will need to coat the substrate with nickel before electroplating Pt black. The cleaning process was conducted by sonicating the substrate successively in Acetone, D.I. water, Ethanol, IPA, 10% Sulfuric Acid and finally D.I. water again each for 5 minutes and then briefly dried with air gun. [64] Cleaning is a very important step in preparing the surface for Nickel and eventually Pt black deposition. In Figure 3.6.a you can see a stainless steel substrate which is not properly cleaned and after Pt

deposition, as you can see in Figure 3.6.b, failure to clean the substrate properly will result in a very poor quality deposition.

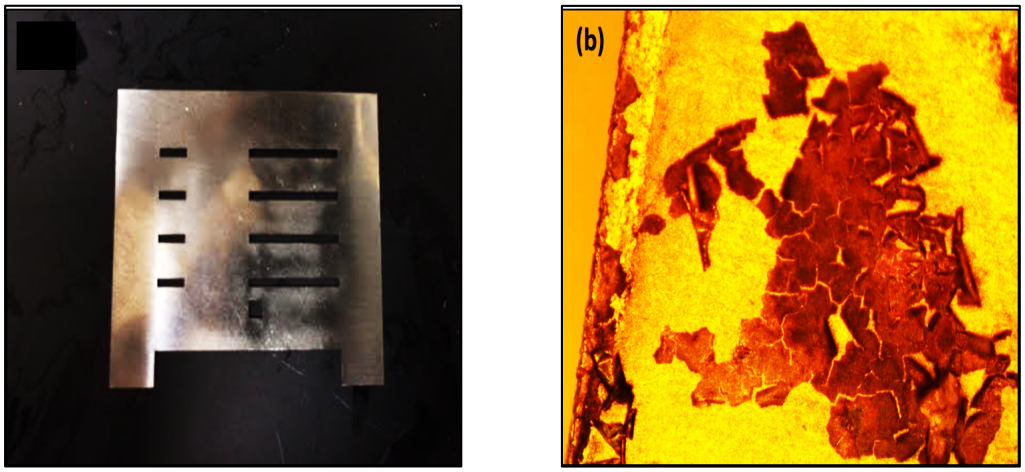

(a) Stainless steel substrate

(b) Magnified view of poorly cleaned surface after Pt deposition

Figure 3.6. Importance of cleaning the substrate

Wood's Nickel Strike [65]

As mentioned before, in order to improve the adhesion between Pt black and the stainless steel substrate, we preformed the Wood's Nickel Strike (WNS) on the substrate. Basically, in this method, a set up similar to galvanic cell is constructed where anode is a thin film of nickel, cathode will be our stainless steel substrate. For the electrolytic solution, a WNS solution containing 240 g/L of $NiCl_{2.6}H_2O$ and 125 g/L HCl was used (Gold Plating Services, Layton, UT). After the substrate was cleaned properly, a double-sided tape was used as the mask for the deposition process, since we only want nickel and eventually platinum only inside the channels. After the substrate was masked using a polyimide double-sided tape, it was connected to the cathode side by clamp as the nickel film is connected to anode with another. As we mentioned before, we used a conventional three-electrode method. The reference

electrode of choice in our study is silver chloride electrode (Ag/AgCl) that will also be placed inside the solution with anode and cathode. To control the current an Arbin Instruments BT-2043 battery testing station was programed to produce current density of 200 A/m^2. Since we have 4 rectangular channels with total area of 36 mm^2,

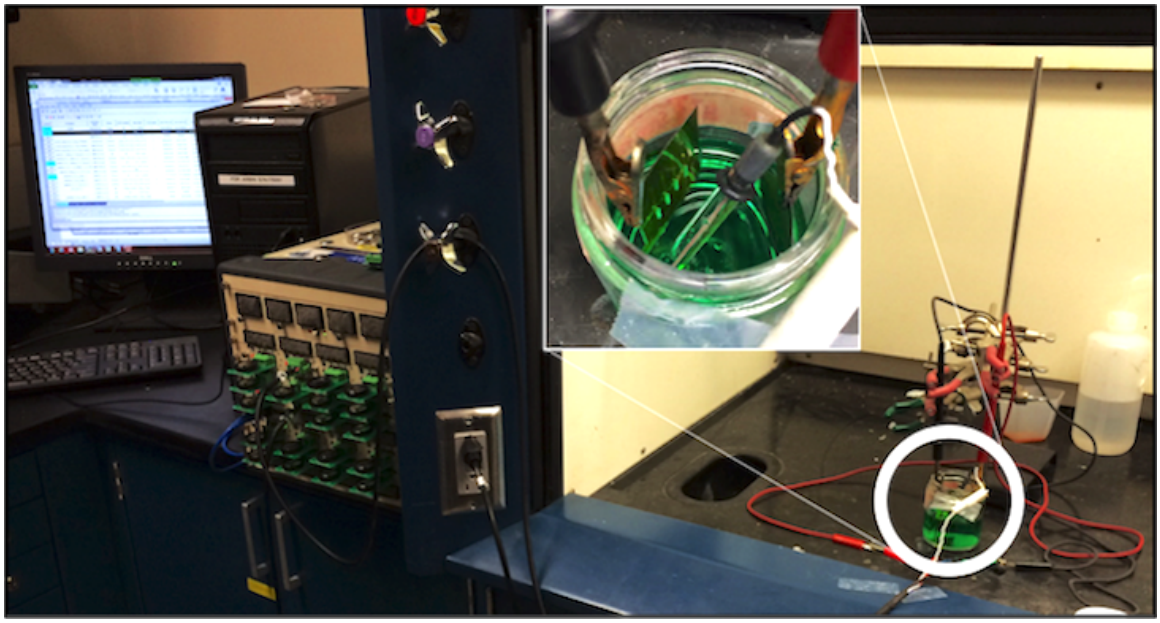

Figure 3.7. Three-electrode setup for Wood's Nickel Strike

The current input on the current generator was set to be 0.0072 A for a duration of 90 seconds (you can see the setup in Figure 3.7). Then we took the substrate out of the solution and rinsed it with D.I. water and then dried it with an air gun. We kept the mask on the substrate since we needed it for Pt electroplating.

After the nickel layer was deposited on the substrate, it was time to electroplate Pt black on the substrate. The process was very similar to the Wood's Nickel Strike. We still had the three-electrode set up (as shown in Figure 3.8.a) and substrate was connected to the cathode while the anode this time was a platinum film and the solution was made of 120 ml of DI water, 5 g of dihydrogen hexachloroplatinate ($H_2PtCl_6 \cdot 6\,H_2O$, Alfa AESAR) and 30 mg of lead acetate ($Pb(CH_2COOH)_2 \cdot 3\,H_2O$,

Alfa AESAR). When the setup was ready, a current density 0.4 A/cm^2 ran through the system for 30 seconds to deposit high surface area platinum inside the channels and on the stainless steel substrate as shown in Figure 3.8.b.

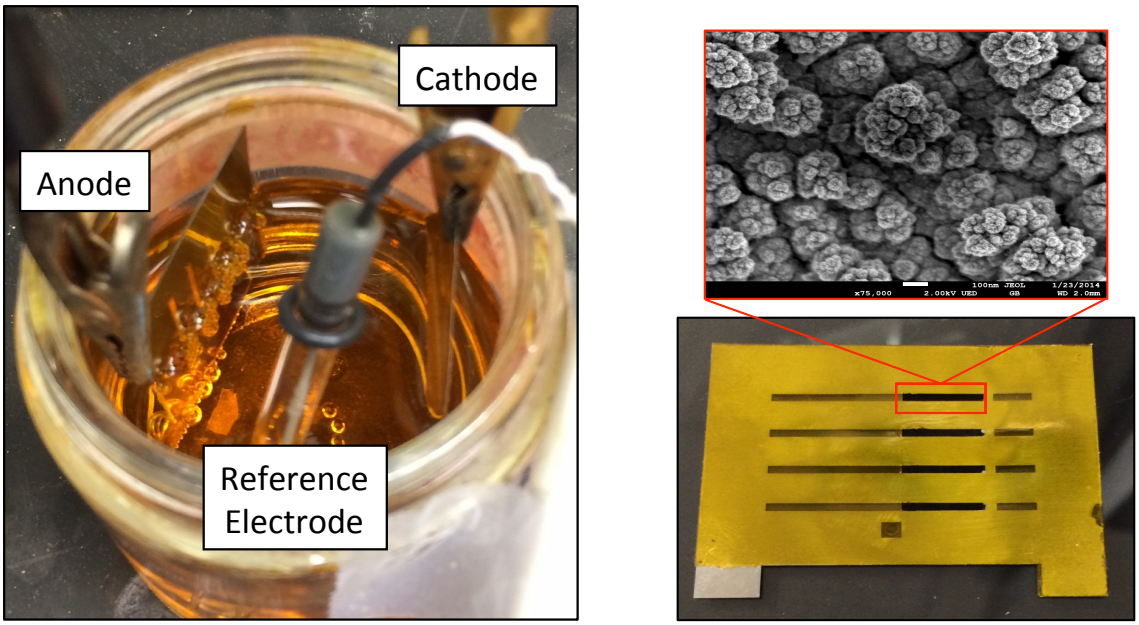

(a) Three-electorde electroplating setup

(b) SEM image of electroplated Pt

Figure 3.8. Electroplating setup and result

The area density of electroplated Pt black was calculated to be 12.1 mg/cm^2. After deposition, the substrate was rinsed in D.I. water and dried in room temperature and the double-sided tape was removed after the substrate was completely dry. The amount of deposited platinum was calculated below and compared by the amount we measured by placing the substrate on a scale before and after Pt deposition. The weight of Pt was measured to be 4.5 mg. There might be a difference between the amount of Pt inside the channels and the one measured by the scale. This difference is due the shape of the mask. Since the mask did not cover the edges of the substrate,

Pt black will be deposited on the edges which does not contribute any issue to the design or our testing results.

$$Area = 9\ mm^2 = 0.09\ cm^2\ for\ 1\ channel$$

$$For\ 4\ channels = 0.09 \times 4 = 0.36\ cm^2 \longrightarrow Area\ deansity = 12.1\ mg/cm^2$$

$$For\ 1\ channel \longrightarrow 0.09 \times 12.1 = 1.089\ mg\ Pt\ per\ channel$$

$$Pt\ density = 21.45\ g/cm^3 \longrightarrow \frac{0.001089}{21.45} = 0.00005056\ cm^3\ (Pt\ volume)$$

$$Pt\ thickness\ inside\ the\ channels = \frac{0.0005056}{0.09} = 0.000562\ cm = 5.62\ microns$$

The platinum thickness inside each channel was calculated to be 5.62 microns. We expected the thickness to be higher than this value but due to the porous structure of the electroplated Pt black the thickness will less than expected.

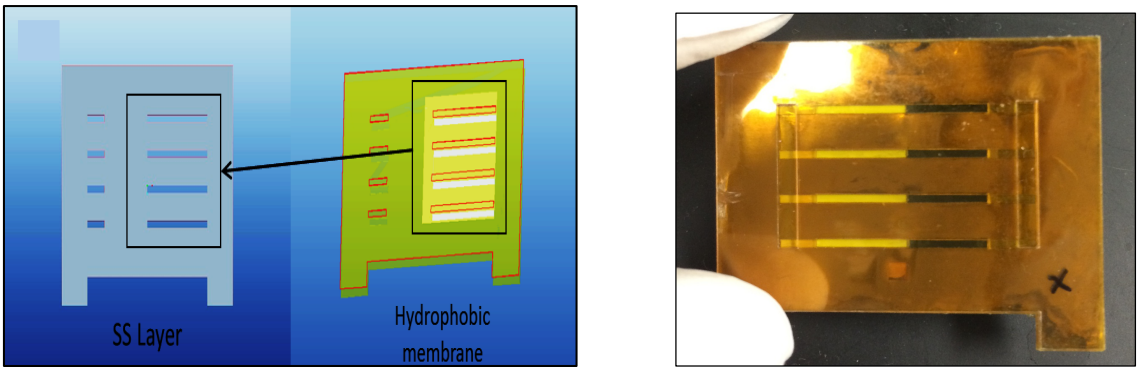

(a) Sanwiched porous hydrophobic membrane's location on the SS layer

(b) Fabricated layers

Figure 3.9. Details of the last layer and final product

When all layers are ready, we can assemble the hydrogen generator. We have already bonded the first two PS layers, now we need to bond the stainless steel layer to the PS layers by double-sided tape. The last step to finish the fabrication, is adding a porous hydrophobic membrane for gas venting. For this purpose we used a PTFE porous membrane (Sterlitech, PTU022550). We first cut the membrane in rectangular shape which is slightly larger than the rectangular gas venting opening.

We sandwiched the membrane between two layers of double-sided tape and bond it to the bottom of the stainless steel layer as you can see in Figure 3.9.a. In Figure 3.9.b you can observe the final product.

Now the hydrogen generator is fabricated and ready to be tested. But before we move on with the testing we need to make sure it meets the channel conditions we discussed in Chapter 1. We can see in the asymmetric schematics of our channels (Figure 3.10) that the check valve (channel neck) and gas venting system meet the requirements explained in Chapter 1. AB solution will enter through the inlet and as it enters the channels, it comes in contact with the Pt black catalyst that has been electroplated inside the channels. As a result bubbles of hydrogen will be created. The check valve will only allow the bubble to grow to the right side due to previously discussed capillary pressure. As more bubbles are generated they will push each other rightward until the reach the porous hydrophobic membrane where they will be vented out due to the bubble trap caused between hydrophilic channels and hydrophobic membrane.

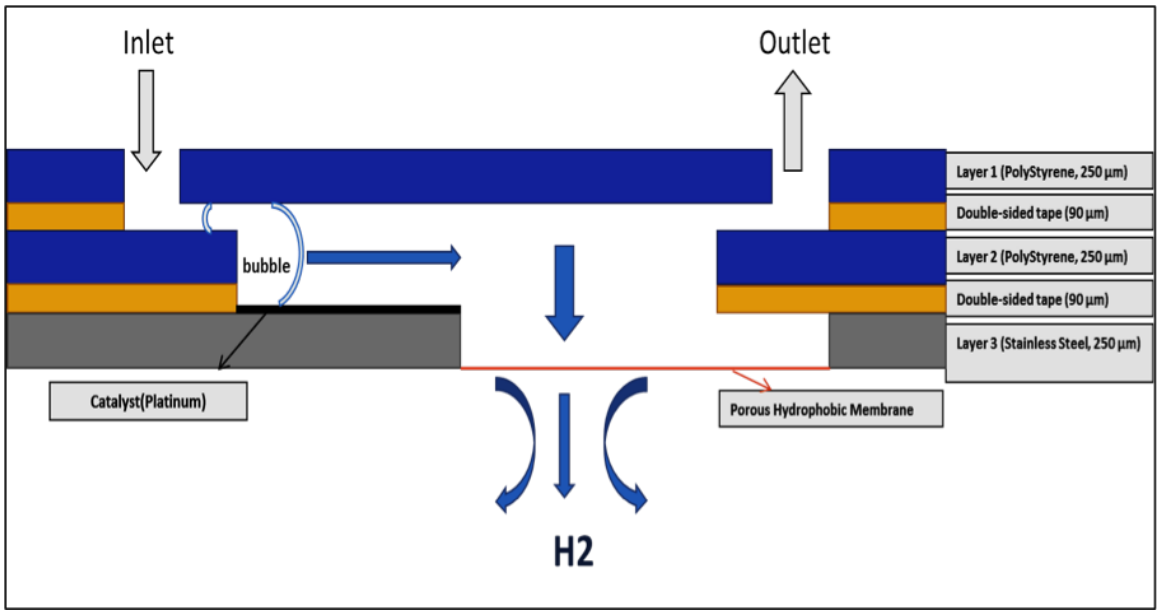

Figure 3.10. Asymmetric channel structure: directional bubble growth and venting

3.3 Fuel Cell

After fabricating the Hydrogen generator, the next step is fabricating the fuel cell we are planning to integrate with it and make sure the fuel cell design works properly. As we mentioned before the heart of the fuel cell is MEA. We used a $1cm^2$ square shaped MEA (60% Pt/C-FuelCellsEtc.com) with GDL included (Carbon cloth). We used hard Teflon (PTFE film made with Teflon fluoropolymer-FuelCellStore) as the gasket for sealing purposes. The teflon gasket was cut manually using a razor. The last pieces for the fuel cell are current collectors. Our current collectors were made of stainless steel with a circular opening of 4mm diameter for Hydrogen entrance on the anode and Oxygen on the cathode side. The current collectors were cut using wire electrical discharge machining to ensure precision. You can see the fuel cell testing package in Figure 3.11.

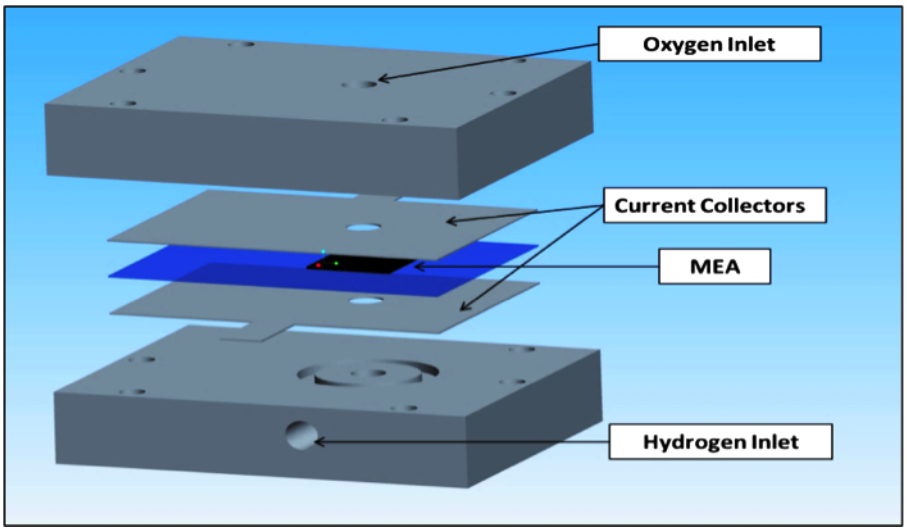

Figure 3.11. Fuel cell testing package

Two blocks of polycarbonate were used for the bottom and top side of the package. Hydrogen is pumped through the inlet and oxygen is breathed from the ambient air. To ensure complete sealing, an O-ring space was created on both top and bottom

blocks. By applying pressure through fastening six screws, the fuel cell was sealed completely.

3.4 Integrated Fuel Cell and Hydrogen Generator Assembly

As the layer by layer computer model of the final package is shown in Figure 3.12.a, hydrogen generator will be bonded to the anode side current collector via double-sided tape. The top and bottom layer of the package are made of transparent polycarbonate. Two holes of 3mm diameter are drilled for the inlet and outlet of the solution on the top layer. The bottom layer has a 1cm diameter opening for oxygen breathing. There are four holes drilled on the corner of the polycarbonate blocks for screws that will hold the package together.

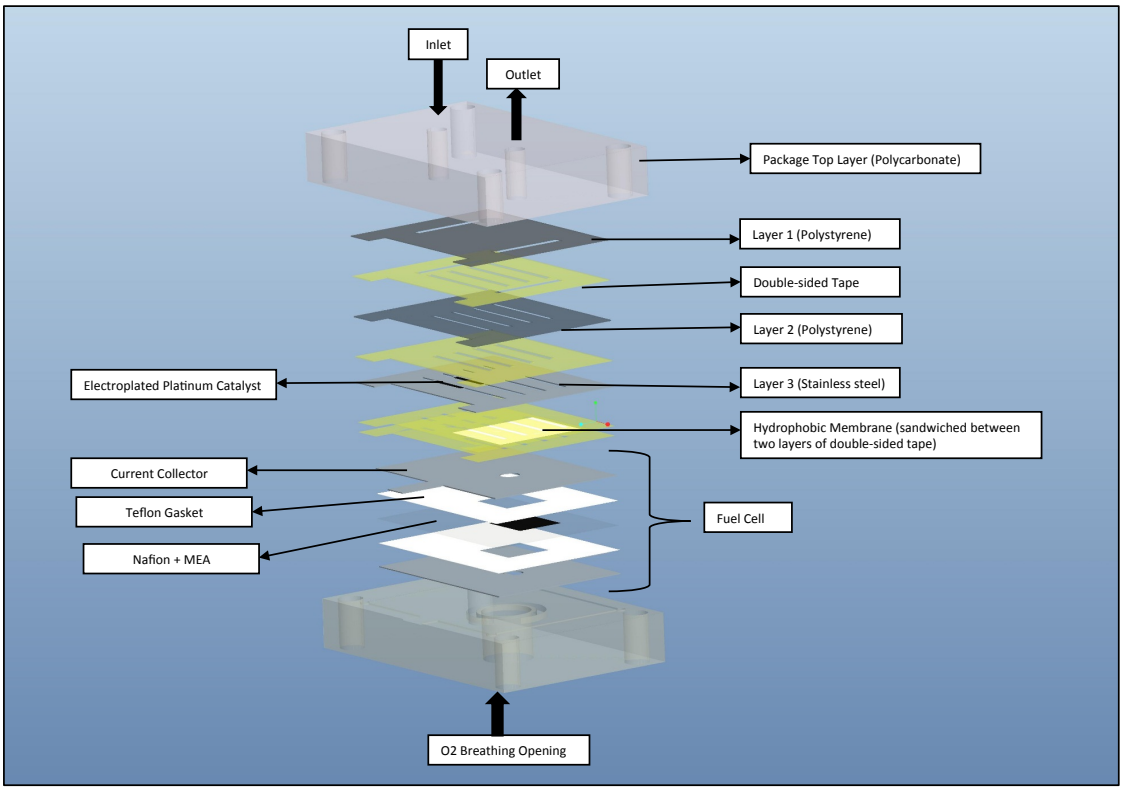

(a) Layer by layer computer model

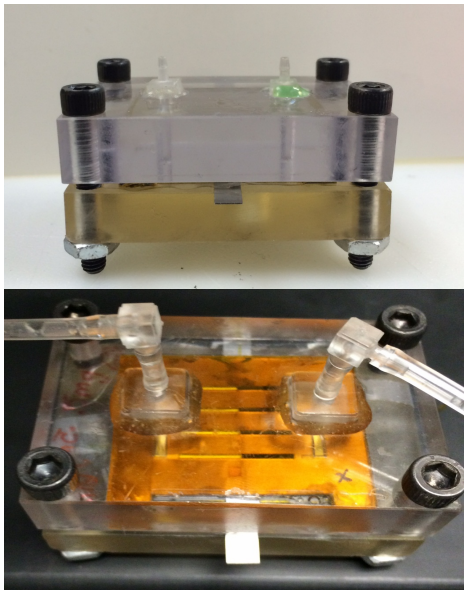

(b) Final product

Figure 3.12. Computer model and final package design

4. RESULTS AND DISCUSSION

The electrochemical surface area of the platinum black in the microchannel was measured in a standard three-electrode cell. The cyclic voltammogram for CO oxidation is shown in Figure 4.1.

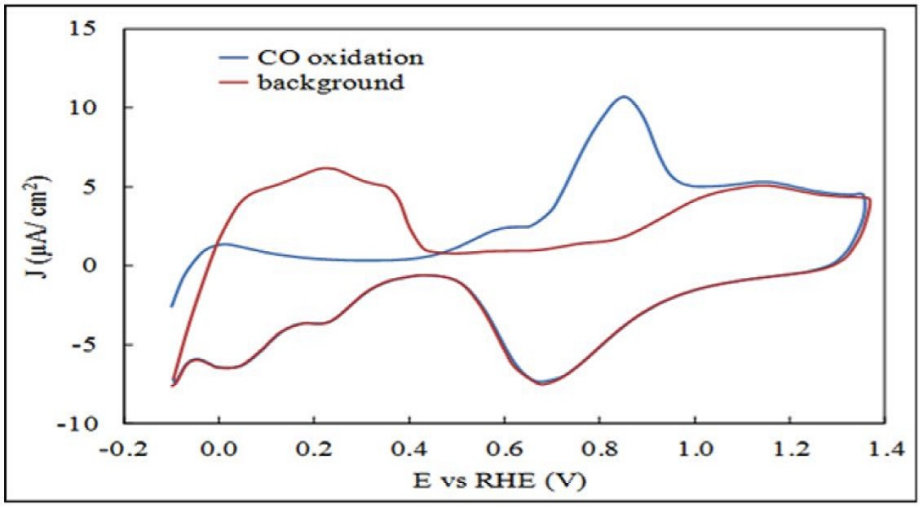

Figure 4.1. Cyclic voltammograms for CO oxidation of nanostructured Pt black catalyst in the microchannel

In this experiment, 0.1 M H_2SO_4 was used as the supporting electrolyte and the solution was saturated with gaseous CO while holding the potential at 57 mV vs. the reversible hydrogen electrode (RHE). The solution was then degassed with argon while maintaining potential control. The potential was then scanned positively at 10 mV/s until the CO was completely removed from the surface. The electrochemical surface area was calculated using the assumption that the linearly adsorbed monolayer of CO would require 420 mC/cm^2 to oxidize. The active surface area of the platinum black is thus calculated to be 69 cm^2. Compared to the geometrical surface area of the reaction microchannels (0.285 cm^2), the active surface has been increased 242

times. Due to the large active surface area of macro- and mesoporous platinum in the microchannels, fast hydrolysis reactions can be achieved in this device.

First, we will only test the hydrogen generator without integrating it with the fuel cell to get the results for gas generation. We used two different solutions each with two different concentrations: ammonia borane in D.I. with 2% and 4% concentrations and hydrogen peroxide in D.I. water with 4% and 8% concentrations. Second, we integrated the hydrogen generator with the fuel cell. Next, we ran multiple tests to study the behavior of the fuel cell before and after integration.

4.1 Hydrogen Generator Results

Ammonia Borane (Sigma Aldrich-97% NH_3BH_3) powder was mixed with D.I. water to create 2% and 4% AB solutions. The same procedure was applied to dilute 30% Hydrogen Peroxide (Fisher Scientific) to create 4% and 8% Hydrogen Peroxide solution. Before injecting solutions into the system, we had to modify our original package design to be able to make sure while we test the hydrogen generator only, there will not be any leakage and only hydrogen (in AB case) and Oxygen (in hydrogen peroxide case) is measured. In order to achieve that, a 0.5 mm layer of polycarbonate was cut to dimension of our layers with the matching opening as our gas venting area as shown in Figure 4.2.a. An inlet was then bonded to the polymer layer via epoxy to make sure there is no leakage on the gas outlet. In order to make sure there will not be any back pressure in the system to create any errors, we kept the pressure the same in both inlet and outlet by using L-shape connectors as shown in Figure 4.2.b. Before testing AB solution, all the tubes and system was purged with Hydrogen gas to minimize the error. Then, Solution was injected in to the system using a syringe pump (KD Scientific-KD 200) with a relatively slow speed (120 μl/hr) and the pumping was stopped and syringe was disconnected as soon as the solution reached the outlet. The volume of injected solution is almost 215mm^3. When we stop the pumping, we observe that the bubble growth mechanism, check valve and venting

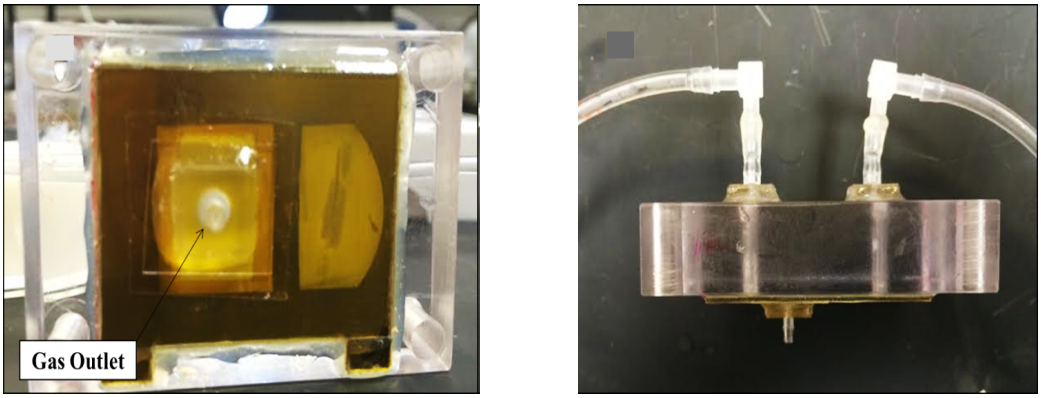

(a) Modified package

(b) L-shape connectors to eliminate back pressure

Figure 4.2. Modified device to measure gas generation rate

membrane are working as predicted as shown in Figure 4.3 (the pictures were taken from the video of the reaction at 4 different times). We can see the produced bubbles of hydrogen as a result of AB solution and Pt black reaction are grown to the right side and eventually vented out of the system.

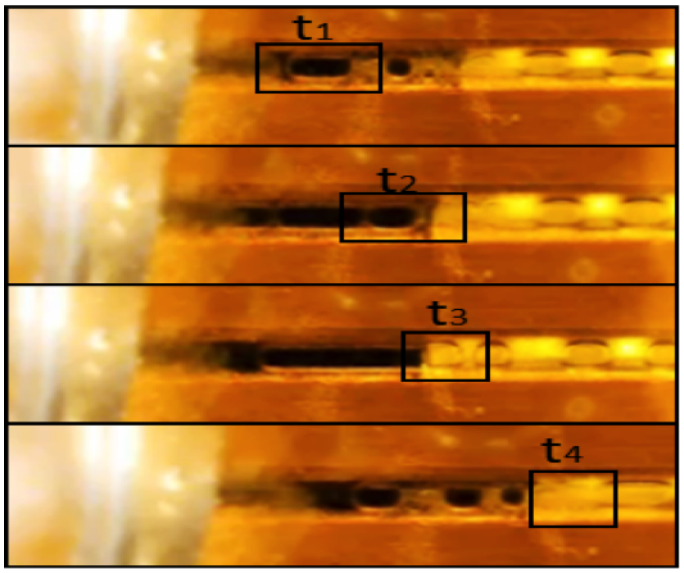

Figure 4.3. Self-circulation bubble-driven Pump at four different times

4.1.1 Gas Generation Rate

Gas generation rates were measured by a mass flow meter (FMA 1600A-Omega). The hydrogen generation profiles for 2% and 4% AB solution are shown in Figure 4.4. Hydrogen generation for both concentrations of AB starts at an almost similar value and drops relatively steadily. The drop can be explained to be the product of decreasing concentration inside the reaction channels as the reaction progresses. The reaction comes to a complete stop after almost 7620 seconds for 2% AB solution and 14400 seconds for 4% concentration. We expected less gas generation for hydrogen peroxide in comparison with AB solution.

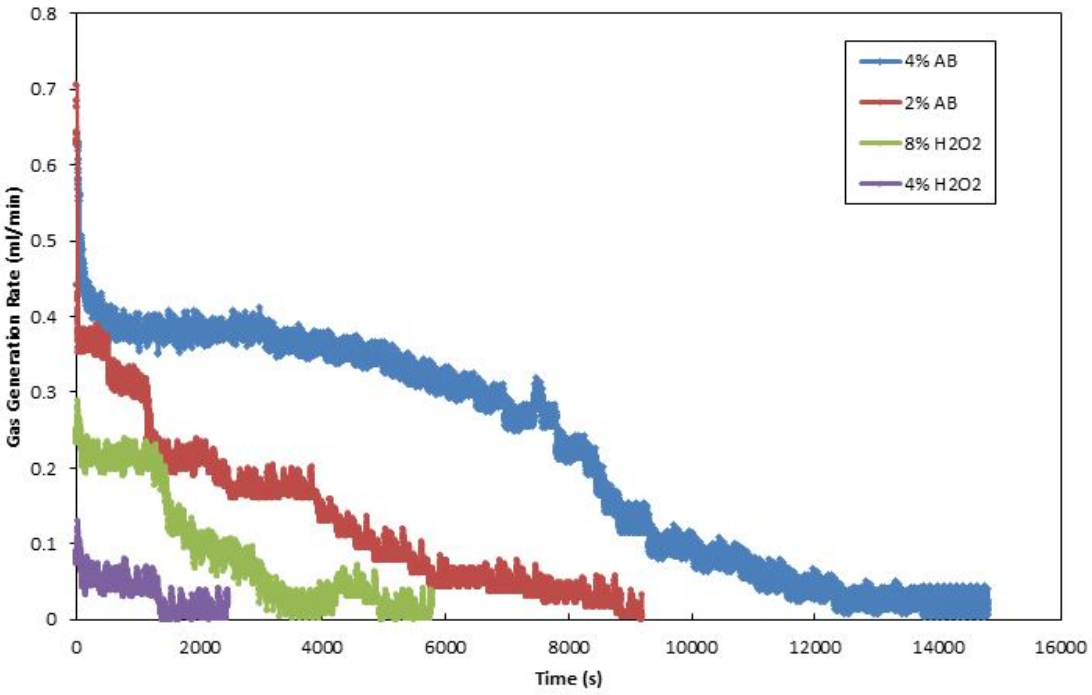

Figure 4.4. Gas generation profile for AB and hydrogen peroxide

Since, assuming STP, for an equal mass of "m" for both material the amount of theoretical hydrogen production will be:

$$\textbf{4\% AB: } \textit{Theoretical } \mathrm{H_2} \textit{ volume} = \frac{m\ (g) \times 4\%}{30.865\ (g/mol)} \times \frac{3\ mol\ \mathrm{H_2}}{1\ mol\ \mathrm{NH_3BH_3}} \times$$

$$22.4\ (l/mol) = 87.08 \times m\ (ml) \tag{4.1}$$

$$\textbf{4\% } \mathbf{H_2O_2}\textbf{: } \textit{Theoretical } \mathrm{O_2} \textit{ volume} = \frac{m\ (g) \times 4\%}{34.01\ (g/mol)} \times \frac{0.5\ mol\ \mathrm{O_2}}{1\ mol\ \mathrm{H_2O_2}} \times$$

$$22.4\ (l/mol) = 13.2 \times m\ (ml) \tag{4.2}$$

Therefore, in an ideal condition, for the same amount of mass and concentration AB produces 6.6 times more hydrogen than hydrogen peroxide (HP) produces Oxygen. For 8% HP solution the oxygen generation rate starts at about 0.3 ml/min while for 4% the value is almost half. From Figure 4.4, we can observe that for 8% HP solution gas generation rate starts at 0.3 ml/min while 4% HP solution starts at 0.14 ml/min. They both have almost similar profile, where in 8% HP gas generation is stable for 600 seconds around 0.2 ml/min before it drops and eventually the reaction stops after almost 5040 seconds. In 4% HP, the short stability occurs at 0.75 ml/min before the generation drops and reaction comes to a complete stop after close to 2520 seconds. As we expected from Equations 4.1 and 4.2, gas generation profiles for both material confirm the equations while AB solutions concentrations produce more hydrogen than HP solutions produce oxygen.

4.1.2 Self-Regulation

In order to verify the Self-regulation of a liquid pumping rate, another testing condition was set up to measure liquid flow rate at various gas venting rates, which will mimic the hydrogen consumption of a fuel cell. The set up was very similar to the previous test, but in order to control the gas flow rate we used a mass flow controller (FMA-700A, Omega) to be able to control the gas flow rate. The gas-venting outlet was connected to the inlet of the controller and gas generation rate

was kept constant at various values (from 50 μl/min to 400 μl/min). Then a tube was marked carefully in intervals of 1mm to act as a ruler. The displacement of the outlet liquid meniscus was recorded by a digital camcorder. Since we know the tube diameter used in this experiment (1.6mm) and the displacement of the meniscus, the liquid pumping rate was then calculated from the velocity of the outlet liquid meniscus. The data for both AB and HP are shown in Figure 4.5. For each material and concentrations' gas generation rate, four measurements of liquid pumping rate were done.From the figure we can observe that liquid pumping rate is regulated by the gas venting rate. When higher gas venting rates are experienced by the system, the liquid circulation rate increases to deliver the needed amount of liquid for the reaction. The maximum hydrogen generation of 0.4 ml/min was achieved with 4% AB solution

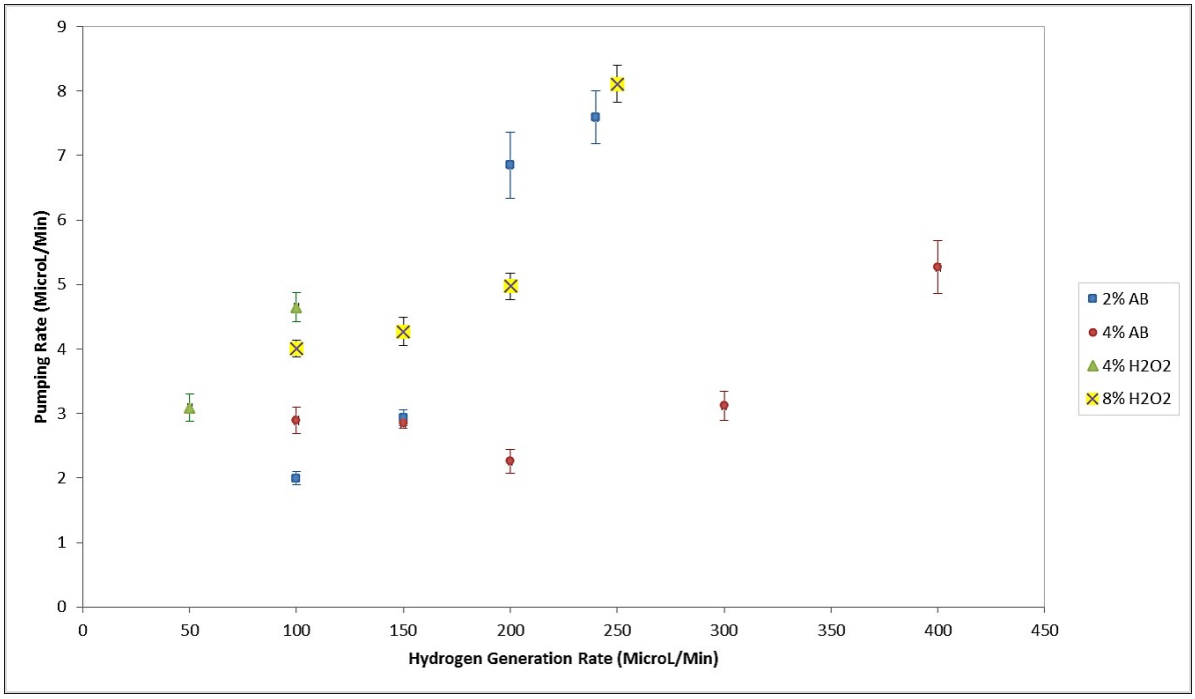

Figure 4.5. Self-regulation of liquid pumping rate by gas generation (venting) rate for various concentrations of HP and AB

which correlates to the liquid pumping rate of $\sim$ 5.1 microl/min.The figure also shows

that lower concentrations of AB (2%) and HP (4%), have higher liquid pumping rate in the same gas venting rate compared to the higher concentration solutions. This data indicates that the gas generator adapts to the concentration of the reactant to be able to regulate hydrogen generation. At a certain gas venting rate, less amount of high concentration reactant is needed and as a result smaller portion of the pumping capability is used. But in the case of lower concentration reactant, the liquid pumping rate should be faster in order to deliver enough reactant in the channels to meet the need for the gas consumption. This effect can also be visually confirmed when we observed that fewer channels are utilized to generate hydrogen for 4% AB solution (three active channels) compared to 2% AB solution (all four channels are active) when hydrogen generation rate was kept constant at 200 μl/min as shown in Figure 4.6.

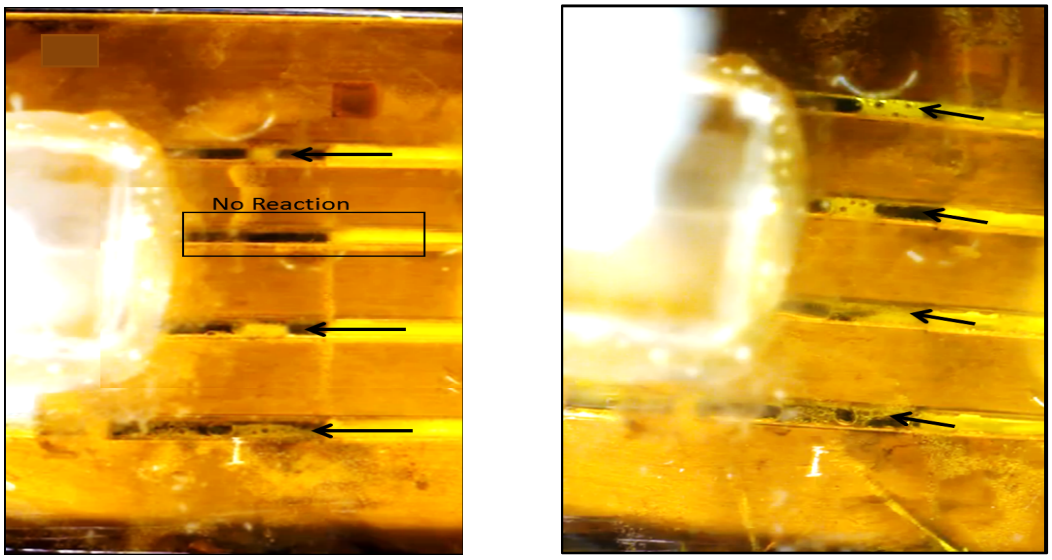

(a) Three channels are pumping liquid (4% AB)

(b) Four channles are actively pumping (2% AB)

Figure 4.6. Snapshot of reaction channels for different AB concentrations

4.1.3 Pressure Head

A setup identical to Figure 4.7 was constructed to measure the pressure head that can be sustained by the device vs the liquid pumping rate.

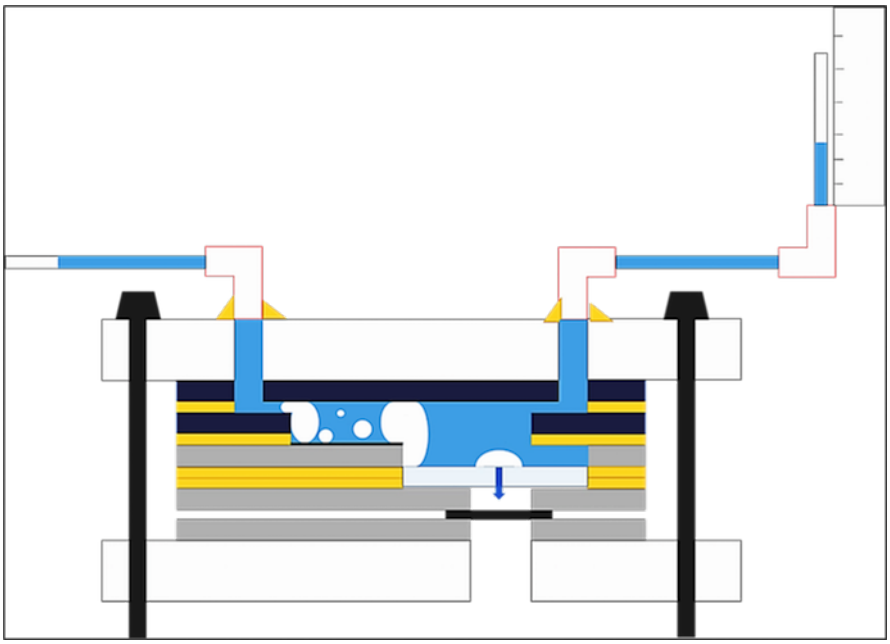

Figure 4.7. Schematics of the device setup for pressure head measurement

The height of the liquid in the vertical tube was measured using a ruler as a function of the time while the experiment was being recorded. The pressure (Pa) was calculated using liquid height inside the tube and liquid characteristics. The velocity of the meniscus moving up in the vertical tube is a representative of liquid pumping rate (μl/min). The experiment was conducted using 2% AB solution. The data points were collected for each time that the meniscus moved 1mm in the outlet tube. 10 data sets were gathered as shown in Figure 4.8. For each data point 4 sets of values were measured and the error bars added to display the spread within one standard deviation from the mean data point. A maximum pumping rate of 7.5 μl/min for liquid pumping rate and maximum pumping head 82 Pa were observed which shows

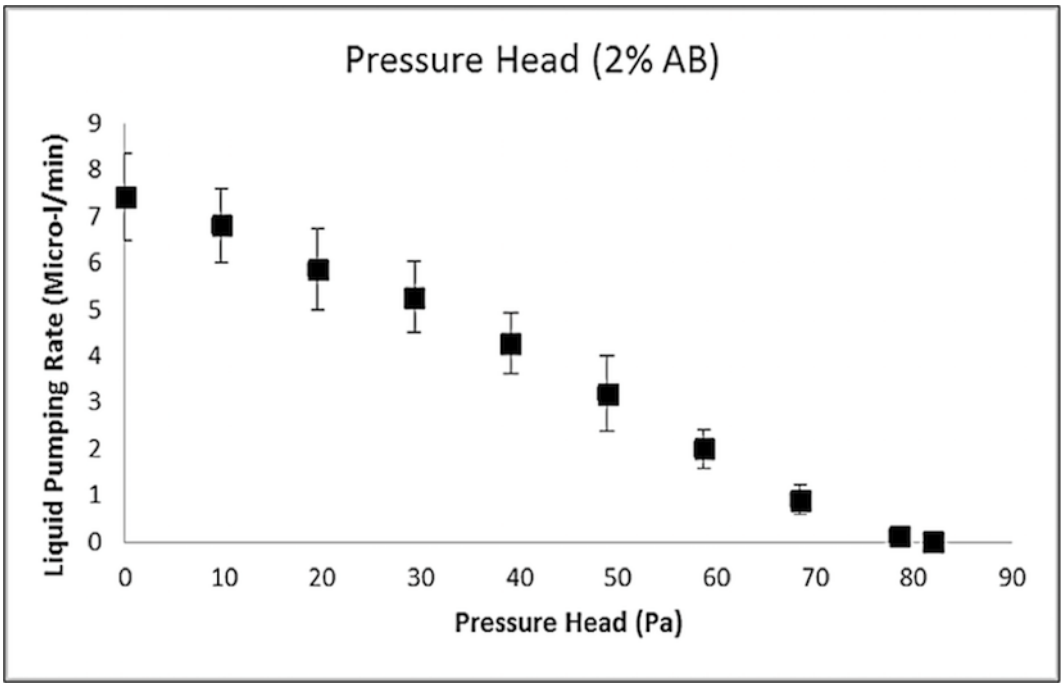

Figure 4.8. Liquid pumping rate versus pressure head for 2% AB

the capability of the device to pump liquid and to deliver 82 Pa of pressure head without suffering from parasitic power consumption.

4.2 Integrated Micro Fuel Cell

After the test is done with the gas generator, we move on to integrate the device with the fuel and analyze the results.

4.2.1 Polarization Curve

Finally, we will test the device as one package with integrated fuel cell. Before running the liquid inside the system, the package was purged with hydrogen gas for 30 minutes. As the device was being purged, we gathered fuel cell's polarization data (voltage versus current density) to have the benchmark of what is the maximum capability of the device when the fuel cell is integrated. Figure 4.9 shows the polarization

and the power density curves of the fuel cell. The fuel cell is capable of producing a

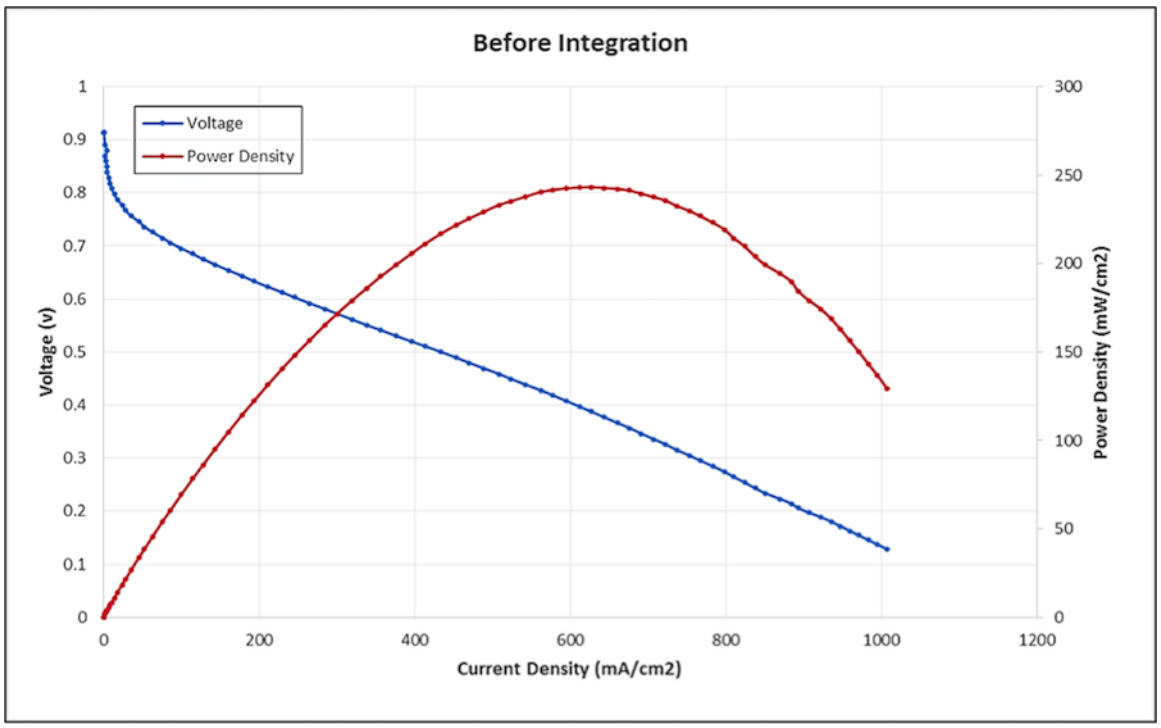

Figure 4.9. Fuel cell polarization and power density curves as being purged with hydrogen

peak power density of 250 mW/cm^2 and is able to generate current density of more than 1000 mA/cm^2 at lower voltage of 0.1 V. After the device is purged with hydrogen, we can start injecting the AB solution in to the system. Figure 4.10 shows a comparison of polarization and power density plots of the integrated fuel cell for 4% and 2% AB solution. The results show the effect of integrating the fuel cell with an onboard hydrogen generator on the performance of the system. Since in our design, fuel cell breathes oxygen from the ambient air, the performance of the device and fuel cell depends solely on the availability of hydrogen at anode. In the unintegrated device, the activation region starts at open circuit and extends to 0.8 V and then starts ohmic behavior with the peak power density occurring at 0.4 V. While in both cases of 4% and 2% AB solution we witness a much abated performance. In both

concentrations, we witness an extension in the activation behavior. For 4% AB, the activation loss drops to 0.75 V with 50% dropping of current density while for 2% AB, the activation loss extends to 0.7 V with 70% drop in current density. This change in behavior is directly connected with the differences in hydrogen availability for each condition. When device is connected to the hydrogen source, the MEA is able to sustain the reaction at cathode and anode at every instant and the hydrogen is delivered at the required partial pressure demand of the MEA.

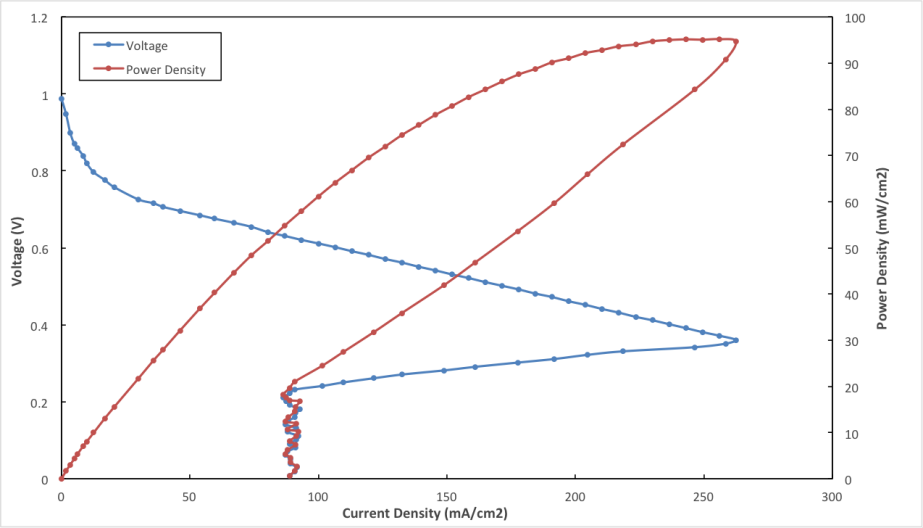

(a) 2% AB solution

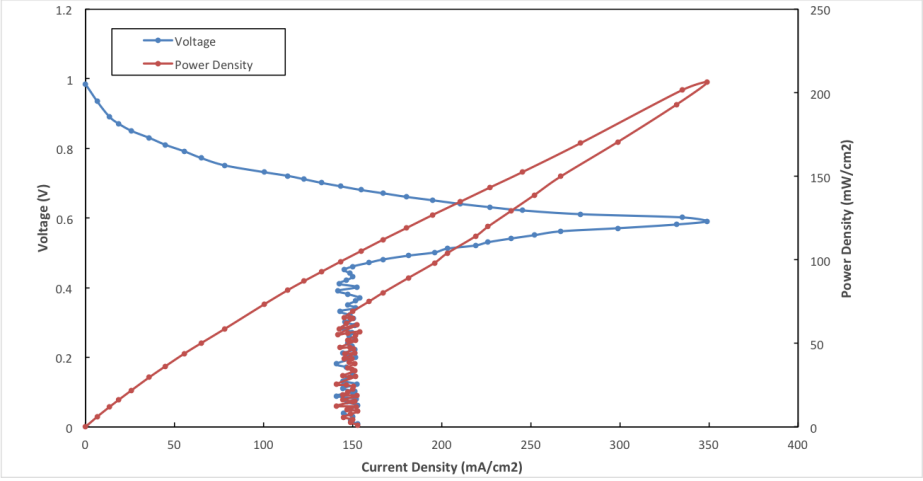

(b) 4% AB solution

Figure 4.10. Polarization plot for integrated device for various AB concentration

While in the integrated device, hydrogen availability is much less than the hydrogen source. This can be even better understood when we compare the two concentrations results. Higher concentration of solution results in relatively better performance at relatively higher current densities. Our virtual check valve can adjust to the fuel cell need for more hydrogen at different current density rates but the amount of liquid available in the channels has a certain limit. Therefore, the design's limit causes more activation loss.

In the ohmic region, the drop for integrated device is steeper compared to the unintegrated device. In this region, fuel cell operation is function of both flow rate and pressure. In the unintegrated device, hydrogen is widely available to satisfy both flow rate and pressure while in the integrated device as we discussed previously we are dealing with a limited rate of hydrogen generation. The other major difference between two devices in this region is when mass transport region starts. In the integrated device, mass transport limit occurs much earlier compared to the unintegrated device. Proton transportation in the MEA is a fast process and as the need for hydrogen increases (as voltage drops) this process needs to be done even faster and this need should be satisfied by pumping liquid at the higher rates and partial pressure. The rate of liquid pumping and the reaction between the liquid and catalyst in order to produce hydrogen is much slower in the integrated device and the reactor is unable to fulfill the hydrogen need at the partial pressure required by the MEA. Therefore, the MEA tends to switch to a mass transport limit region and loses efficiency. The ohmic region extends to 0.39 V for 2% AB solution with the peak power density of 95 mW/cm^2 while for 4% AB solution the mass transport limit occurs at 0.6 V with a higher peak power density at 215 mW/cm^2.

Integrated device is completely mass transport limited under a certain voltage (0.39 V for 2% AB and 0.6 V for 4% AB solution). In this region, the MEA reaction rates are so fast that any generated hydrogen molecule that comes close to the MEA is immediately oxidized and ions transport in a very high speed. When MEA is fed enough hydrogen, it will be able to deliver high current densities but the integrated

device even at its performance limit, is unable to fulfill the MEA need to produce high current density. As you can see while the unintegrated device is able to produce relatively high current density of more than 1000 mA/cm^2, the integrated device can produce maximum of 350 mA/cm^2 with 4% AB solution.

The mass transport limitation causes the skewed shape in the mass transport limit region where for the same value of current density, there are multiple voltage solutions available. When the fuel cell operates in the low currents, there may be unused hydrogen accumulated in the anode side of the fuel cell while in the higher current density, the device goes to mass transport limit when the accumulated hydrogen is consumed.

4.2.2 Switching of Load and Device Reaction

Performance of the integrated device under varying load for both AB concentrations (2% and 4%) are shown in Figures 4.11 and 4.12. As it can be seen in voltage versus time plot (specified with green dashed line), fuel cell's operating voltage was set as a dynamic square wave, switching between 0.8 V and 0.3 V for 2% AB and between 0.8 V and 0.4 V for 4% AB every 10 minutes. The reason for choosing the voltage values was first, to check devices response in high and low electric loads. Second, to check device's behavior while it is activation limited at higher voltage and fully mass transport limited at lower voltage. As you can see in the figure, the response is in sync with the polarization curves. The value of current density matches the polarization curve data as for both AB concentrations. In both figures, when switching to high electric load, current density experiences a sharp increase in value for a brief moment which is due to the built up hydrogen at high partial pressure at the anode of our fuel cell. This behavior lasted for a brief time of 15 seconds which is the time needed for consumption of surplus hydrogen at the anode. Afterwards, the hydrogen pressure drops to the value at which AB solution is pumped through the micro-channels to supply the fuel cell with the high hydrogen required at low voltage. At this moment,

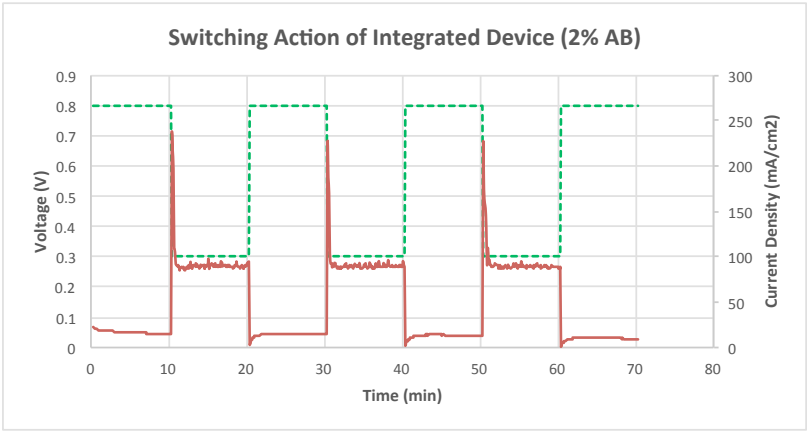

(a) Loaded with 2% AB

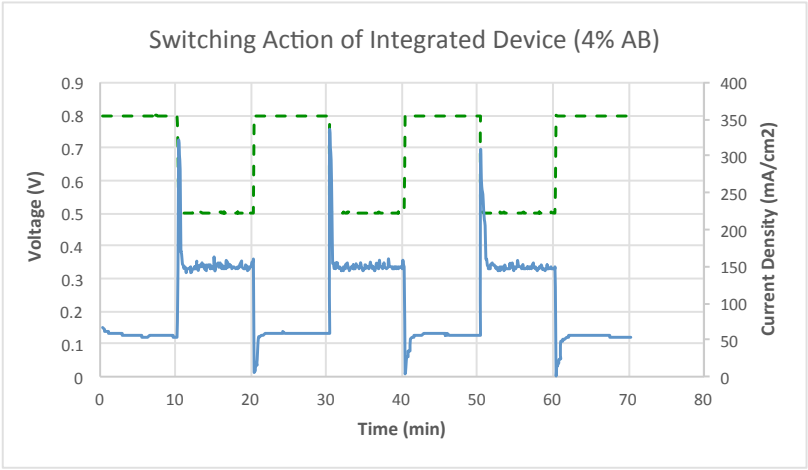

(b) Loaded with 4% AB

Figure 4.11. Switching action of the integrated device

current density drops distinctly to the dwell value for the remainder of the period. As the next period starts (switching from low voltage/high power demand to high voltage/low power demand), the currently density momentarily drops to zero due to the low hydrogen partial pressure. At this moment AB solution is pumped in to the micro-channels to continue hydrogen generation until the MEA's requirements are met and current density value is increased to its dwell value to match the current density requirements at 0.8 V. This causes the hydrogen accumulation at the anode and increases the partial pressure.

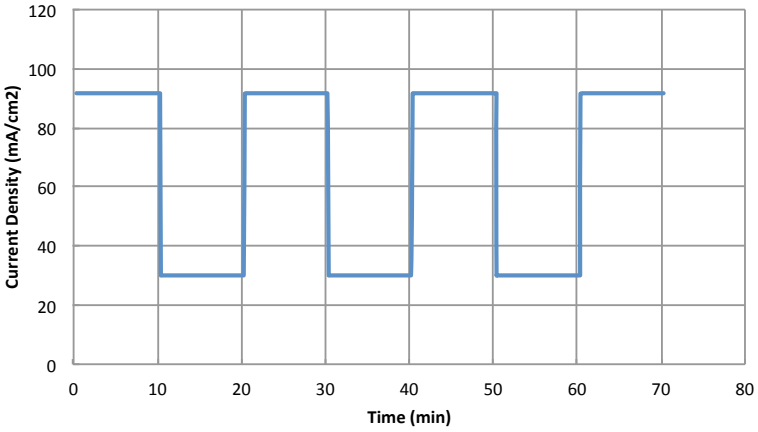

(a) Current density square wave

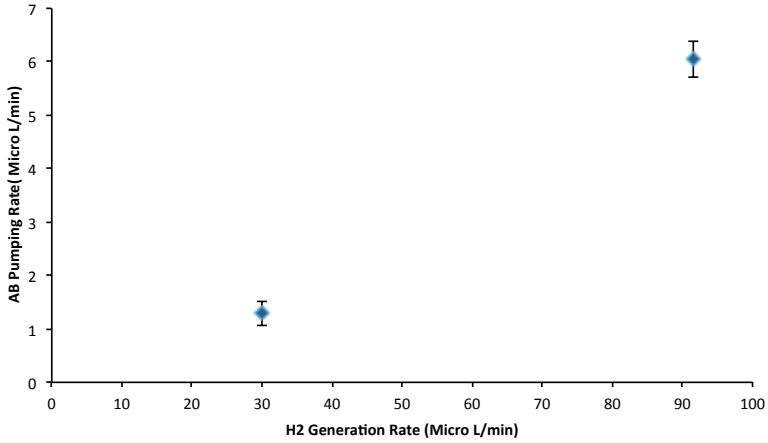

(b) AB solution pumping rate versus hydrogen generation rate

Figure 4.12. Pumping rate of the integrated device while being subjected to a varying current density filled with 2% AB solution

Figure 4.12 shows the 2% AB solution's pumping rate while the integrated device is subjected to varying current densities. Using the testing station, a square wave was set with 10-minute time period. In order to measure the pumping rate, a setup similar to pressure head measurement was used (refer to Section 4.1.3) but this time both inlet and outlet tubes had similar heights to prevent extra pressure. By using a ruler and a timer, we were able to measure the solution's pumping rate. For each

of the two data points, four sets of values were measured and the error bars added to display the spread within one standard deviation from the mean data point. At high current density of 91.58 mA/cm^2, the average pumping rate is 1.297 μl/min and at the lower current density of 30 mA/cm^2, pumping rate average is 6.05 μl/min. In order to analyze the data we need to compare it to Figure 4.5. This will help us to further investigate the integrated device in term of hydrogen consumption efficiency. Therefore, we need to relate current density and hydrogen generation as shown in the following equations.

In fuel cell:

$$\mathrm{H_2} \longrightarrow 2\,\mathrm{H^+} + 2\,\mathrm{e^-}$$

$$1\ A = 1\ C/sec$$

$$moles\ of\ electrons\ per\ second: \frac{1\ C/sec}{96485.3365\ C/mol} = 1.0346 \times\ 10^{-5}\ mol/sec$$

$$mole\ H_2 = \frac{1.0346 \times 10^{-5}}{2} = 40.5182 \times 10^{-5}\ mol/sec$$

At high current density (91.58 mA/cm^2) the average pumping rate is 6.053 μl/min which according to Figure 4.5 corresponds to 189.834 μl/min or 3.163 μl/sec hydrogen generation rate. Therefore assuming STP:

$$91.58\ mA/cm^2 = 11.508\ mA\ (MEA\ area\ = 0.125663\ cm^2)$$

$$\frac{11.508\ mA}{96485.3365\ C/mol} = 1.192 \times 10^{-7}\ mol/sec\ H_2$$

$$1.192 \times 10^{-7}\ mol/sec \times 22.4\ L/mol = 2.671\ \mu L/sec = 160.292\ \mu L/min\ H_2 \quad (4.3)$$

Equation 4.3 shows that hydrogen generation rate at 91.58 mA/cm^2 is 160.292 μl/min. This indicates that about 88.6% of the generated hydrogen was consumed by the fuel cell or in other word, 11.4% of generated hydrogen is wasted by the integrated device and not consumed by the fuel cell. There are many factors that can contribute to the hydrogen waste: in our calculation we have assumed STP conditions at which 1 mole of hydrogen is 22.4 liter and of course this is and ideal assumption. The other factor

might be related to the fuel cell itself. Since our fuel cell breathes outside air for oxygen and we do not have a water recovery system, excess water and nitrogen that may cross the MEA from cathode can decrease the amount of consumed hydrogen at the catalyst surface, which can cause performance losses [66].

5. CONCLUSION AND FUTURE WORK

5.1 Conclusions

The goal of this project is to fabricate an integrated micro PEM fuel cell with self-circulating and self-regulating mechanism using Ammonia Borane as the fuel for hydrogen generation. Integrated device was fabricated using combination of polystyrene and stainless steel. Platinum was electroplated in four micro-channels . The onboard hydrogen generator was first tested separately using different concentrations of Ammonia Borane solution in water (2% and 4%) and Hydrogen Peroxide in water (4% and 8%) and was able to reach a maximum AB pumping rate of $\sim$8.2 μl/min while generating 240 μl/min for 2% concentration and $\sim$5.8 μl/min pumping rate at 400 μl/min hydrogen generation for 4%. For HP, the maximum pumping rate of 8.5 μl/min was achieved while generating oxygen rate was 250 μl/min. Eventually, the hydrogen generator was integrated with a micro PEM fuel cell and a peak power density of 118 mW/cm^2 and 200 mW/cm^2 was achieved by 2% and 4% AB Solutions.

5.2 Challenges and Future Work

The integrated micro fuel cell has been proven and our goals have been achieved. But the performance result of the integrated device showed that there is still a lot of room to achieve perfection. Some of the issues and challenges of the current project that need further investigations are listed below:

- An onboard water recovery system is needed since water/humidity management plays an important role in fuel cell's efficiency. As stated in the previous chapter the crossed over water from cathode can effect hydrogen consumption in anode.

- Catalyst durability is also an issue that needs to be addressed in a long run. Although AB has much better catalyst durability than SB, but gradual reduction in hydrogen generation rate is still an issue with AB [67, 68]. This reduction in hydrogen generation rate can be caused by reduction in catalytic area due to the byproducts (Ammonium and Borate). That is why we need to rinse the channels with DI water after each test to clean the surface of Pt from the byproducts.

- One of the keys to self-pumping of AB inside is hydrophilicity of the channels. As we mentioned in Chapter 2, the top side of the channels are made of polystyrene. Oxygen plasma treatment of PS can last for a certain amount of time. We need to make sure the surface treatment is permanent.

- As we observed in Chapter 4, micro fuel cell is hydrogen mass transport limited that will result in gradual fading of the current density.

- Hydrogen is typically very difficult to store and contain. Due to the relatively small size of the integrated device and its components, hydrogen can leak via onboard gas generator or cross over through the PEM.

REFERENCES

REFERENCES

[1] J. B. Goodenough and Y. Kim, "Challenges for rechargeable li batteries?" *Chemistry of Materials*, vol. 22, no. 3, pp. 587–603, 2009.

[2] R. Kötz and M. Carlen, "Principles and applications of electrochemical capacitors," *Electrochimica Acta*, vol. 45, no. 15, pp. 2483–2498, 2000.

[3] M. Winter and R. J. Brodd, "What are batteries, fuel cells, and supercapacitors?" *Chemical reviews*, vol. 104, no. 10, pp. 4245–4270, 2004.

[4] B. C. Steele and A. Heinzel, "Materials for fuel-cell technologies," *Nature*, vol. 414, no. 6861, pp. 345–352, 2001.

[5] J. W. Weidner, V. A. Sethuraman, and J. W. Van Zee, "Membrane electrode assembly," *Electrochemical Society Interface*, p. 41, 2003.

[6] I. DuPont. (2014, Jun.) Dupont fuel cells. (Last accessed: Aug 2014). [Online]. Available: http://www2.dupont.com/FuelCells/en-US/assets/downloads/dfc101.pdf

[7] C. Wang, M. Waje, X. Wang, J. M. Tang, R. C. Haddon, and Y. Yan, "Proton exchange membrane fuel cells with carbon nanotube based electrodes," *Nano letters*, vol. 4, no. 2, pp. 345–348, 2004.

[8] C. Kim, Y. J. Kim, Y. Am Kim, T. Yanagisawa, K. C. Park, M. Endo, and M. S. Dresselhaus, "High performance of cup-stacked-type carbon nanotubes as a pt–ru catalyst support for fuel cell applications," *Journal of applied physics*, vol. 96, no. 10, pp. 5903–5905, 2004.

[9] H. Tang, J. Chen, L. Nie, D. Liu, W. Deng, Y. Kuang, and S. Yao, "High dispersion and electrocatalytic properties of platinum nanoparticles on graphitic carbon nanofibers (gcnfs)," *Journal of colloid and interface science*, vol. 269, no. 1, pp. 26–31, 2004.

[10] G. Bender, T. A. Zawodzinski, and A. P. Saab, "Fabrication of high precision pefc membrane electrode assemblies," *Journal of power sources*, vol. 124, no. 1, pp. 114–117, 2003.

[11] B. Seger and P. V. Kamat, "Electrocatalytically active graphene-platinum nanocomposites. role of 2-d carbon support in pem fuel cells," *The Journal of Physical Chemistry C*, vol. 113, no. 19, pp. 7990–7995, 2009.

[12] C. Spiegel, *Designing and building fuel cells*. Mcgraw-hill New York, NY, USA, 2007.

[13] V. Ramani, H. R. Kunz, and J. M. Fenton, "The polymer electrolyte fuel cell," *Interface*, vol. 13, no. 3, pp. 17–19, 2004.

[14] J. B. Benziger, M. B. Satterfield, W. H. Hogarth, J. P. Nehlsen, and I. G. Kevrekidis, "The power performance curve for engineering analysis of fuel cells," *Journal of Power Sources*, vol. 155, no. 2, pp. 272–285, 2006.

[15] J. D. Morse, "Micro-fuel cell power sources," *International Journal of Energy Research*, vol. 31, no. 6-7, pp. 576–602, 2007.

[16] G. Lu, C. Wang, T. Yen, and X. Zhang, "Development and characterization of a silicon-based micro direct methanol fuel cell," *Electrochimica Acta*, vol. 49, no. 5, pp. 821–828, 2004.

[17] S. Motokawa, M. Mohamedi, T. Momma, S. Shoji, and T. Osaka, "Mems-based design and fabrication of a new concept micro direct methanol fuel cell (μ-dmfc)," *Electrochemistry Communications*, vol. 6, no. 6, pp. 562–565, 2004.

[18] V. V. Swaminathan, L. Zhu, B. Gurau, R. I. Masel, and M. A. Shannon, "Integrated micro fuel cell with on-demand hydrogen production and passive control mems," *Microfluidics and nanofluidics*, vol. 12, no. 5, pp. 735–749, 2012.

[19] A. Kundu, J. Jang, J. Gil, C. Jung, H. Lee, S.-H. Kim, B. Ku, and Y. Oh, "Micro-fuel cells?current development and applications," *Journal of Power Sources*, vol. 170, no. 1, pp. 67–78, 2007.

[20] Z. Xia and S. Chan, "Feasibility study of hydrogen generation from sodium borohydride solution for micro fuel cell applications," *Journal of Power Sources*, vol. 152, pp. 46–49, 2005.

[21] J.-H. Wee, K.-Y. Lee, and S. H. Kim, "Sodium borohydride as the hydrogen supplier for proton exchange membrane fuel cell systems," *Fuel processing technology*, vol. 87, no. 9, pp. 811–819, 2006.

[22] T. Kim, "Fully-integrated micro pem fuel cell system with nabh 4 hydrogen generator," *International journal of hydrogen energy*, vol. 37, no. 3, pp. 2440–2446, 2012.

[23] L. Zhu, N. Kroodsma, J. Yeom, J. Haan, M. Shannon, and D. Meng, "An on-demand microfluidic hydrogen generator with self-regulated gas generation and self-circulated reactant exchange with a rechargeable reservoir," *Microfluidics and nanofluidics*, vol. 11, no. 5, pp. 569–578, 2011.

[24] G. Thomas and C. San Ramon, "Overview of storage development doe hydrogen program," *Sandia National Laboratories*, vol. 9, 2000.

[25] Y. Lu, H. Wang, Y. Liu, Q. Xue, L. Chen, and M. He, "Novel microfibrous composite bed reactor: high efficiency h 2 production from nh3 with potential for portable fuel cell power supplies," *Lab on a Chip*, vol. 7, no. 1, pp. 133–140, 2007.

[26] M. Ni, D. Y. Leung, and M. K. Leung, "A review on reforming bio-ethanol for hydrogen production," *International Journal of Hydrogen Energy*, vol. 32, no. 15, pp. 3238–3247, 2007.

[27] P. Muthukumar, M. P. Maiya, and S. S. Murthy, "Experiments on a metal hydride-based hydrogen storage device," *International Journal of Hydrogen Energy*, vol. 30, no. 15, pp. 1569–1581, 2005.

[28] B. Sakintuna, F. Lamari-Darkrim, and M. Hirscher, "Metal hydride materials for solid hydrogen storage: a review," *International Journal of Hydrogen Energy*, vol. 32, no. 9, pp. 1121–1140, 2007.

[29] L. Zhu, D. Kim, H. Kim, R. Masel, and M. Shannon, "Hydrogen generation from hydrides in millimeter scale reactors for micro proton exchange membrane fuel cell applications," *Journal of Power Sources*, vol. 185, no. 2, pp. 1334–1339, 2008.

[30] Y. Kojima, K.-i. Suzuki, K. Fukumoto, M. Sasaki, T. Yamamoto, Y. Kawai, and H. Hayashi, "Hydrogen generation using sodium borohydride solution and metal catalyst coated on metal oxide," *International Journal of Hydrogen Energy*, vol. 27, no. 10, pp. 1029–1034, 2002.

[31] R. Oronzio, G. Monteleone, A. Pozio, M. De Francesco, and S. Galli, "New reactor design for catalytic sodium borohydride hydrolysis," *International journal of hydrogen energy*, vol. 34, no. 10, pp. 4555–4560, 2009.

[32] Q. Zhang, G. Smith, Y. Wu, and R. Mohring, "Catalytic hydrolysis of sodium borohydride in an auto-thermal fixed-bed reactor," *International journal of hydrogen energy*, vol. 31, no. 7, pp. 961–965, 2006.

[33] U. B. Demirci and P. Miele, "Sodium borohydride versus ammonia borane, in hydrogen storage and direct fuel cell applications," *Energy & Environmental Science*, vol. 2, no. 6, pp. 627–637, 2009.

[34] A. Al-Kukhun, H. T. Hwang, and A. Varma, "A comparison of ammonia borane dehydrogenation methods for proton-exchange-membrane fuel cell vehicles: hydrogen yield and ammonia formation and its removal," *Industrial & Engineering Chemistry Research*, vol. 50, no. 15, pp. 8824–8835, 2011.

[35] F. Baitalow, G. Wolf, J.-P. Grolier, F. Dan, and S. Randzio, "Thermal decomposition of ammonia–borane under pressures up to 600bar," *Thermochimica acta*, vol. 445, no. 2, pp. 121–125, 2006.

[36] J.-M. Yan, X.-B. Zhang, T. Akita, M. Haruta, and Q. Xu, "One-step seeding growth of magnetically recyclable au@ co core- shell nanoparticles: highly efficient catalyst for hydrolytic dehydrogenation of ammonia borane," *Journal of the American Chemical Society*, vol. 132, no. 15, pp. 5326–5327, 2010.

[37] M. Bowden, T. Kemmitt, W. Shaw, N. Hess, J. Linehan, M. Gutowski, B. Schmid, and T. Autrey, "Mechanistic studies of hydrogen release from solid amine borane materials," in *MRS Proceedings*, vol. 927. Cambridge Univ Press, 2006, pp. 0927–EE02.

[38] M. Chandra and Q. Xu, "A high-performance hydrogen generation system: transition metal-catalyzed dissociation and hydrolysis of ammonia–borane," *Journal of Power Sources*, vol. 156, no. 2, pp. 190–194, 2006.

[39] M. Chandra and Q. Xue, "Room temperature hydrogen generation from aqueous ammonia-borane using noble metal nano-clusters as highly active catalysts," *Journal of Power Sources*, vol. 168, no. 1, pp. 135–142, 2007.

[40] R. P. Shrestha, H. V. Diyabalanage, T. A. Semelsberger, K. C. Ott, and A. K. Burrell, "Catalytic dehydrogenation of ammonia borane in non-aqueous medium," *International journal of hydrogen energy*, vol. 34, no. 6, pp. 2616–2621, 2009.

[41] S. Moghaddam, E. Pengwang, R. I. Masel, and M. A. Shannon, "A self-regulating hydrogen generator for micro fuel cells," *Journal of Power Sources*, vol. 185, no. 1, pp. 445–450, 2008.

[42] V. V. Swaminathan, L. Zhu, B. Gurau, R. Masel, and M. Shannon, "A micro hydrogen generator with a microfluidic self-regulating valve for sensors and fuel cells," in *Micro Electro Mechanical Systems, 2009. MEMS 2009. IEEE 22nd International Conference on.* IEEE, 2009, pp. 35–38.

[43] D. D. Meng *et al.*, "Micropumping of liquid by directional growth and selective venting of gas bubbles," *Lab on a Chip*, vol. 8, no. 6, pp. 958–968, 2008.

[44] D. Meng and C.-J. Kim, "Embedded self-circulation of liquid fuel for a micro direct methanol fuel cell," in *Micro Electro Mechanical Systems, 2007. MEMS. IEEE 20th International Conference on.* IEEE, 2007, pp. 85–88.

[45] E. W. Young, E. Berthier, D. J. Guckenberger, E. Sackmann, C. Lamers, I. Meyvantsson, A. Huttenlocher, and D. J. Beebe, "Rapid prototyping of arrayed microfluidic systems in polystyrene for cell-based assays," *Analytical chemistry*, vol. 83, no. 4, pp. 1408–1417, 2011.

[46] M. Toner and D. Irimia, "Blood-on-a-chip," *Annual review of biomedical engineering*, vol. 7, p. 77, 2005.

[47] H. Becker and C. Gärtner, "Polymer microfabrication technologies for microfluidic systems," *Analytical and bioanalytical chemistry*, vol. 390, no. 1, pp. 89–111, 2008.

[48] S. Guruvenket, G. M. Rao, M. Komath, and A. M. Raichur, "Plasma surface modification of polystyrene and polyethylene," *Applied Surface Science*, vol. 236, no. 1, pp. 278–284, 2004.

[49] D. Zhang, S. Dougal, and M. Yeganeh, "Effects of uv irradiation and plasma treatment on a polystyrene surface studied by ir-visible sum frequency generation spectroscopy," *Langmuir*, vol. 16, no. 10, pp. 4528–4532, 2000.

[50] R. M. France and R. D. Short, "Plasma treatment of polymers: the effects of energy transfer from an argon plasma on the surface chemistry of polystyrene, and polypropylene. a high-energy resolution x-ray photoelectron spectroscopy study," *Langmuir*, vol. 14, no. 17, pp. 4827–4835, 1998.

[51] J. Lai, B. Sunderland, J. Xue, S. Yan, W. Zhao, M. Folkard, B. D. Michael, and Y. Wang, "Study on hydrophilicity of polymer surfaces improved by plasma treatment," *Applied Surface Science*, vol. 252, no. 10, pp. 3375–3379, 2006.

[52] I. KsugaDenki. (2014, Jun.) Principle of surface modification by corona/gas plasma. (Last accessed: Oct 2014). [Online]. Available: http://www.ekasuga.co.jp/en/product/185/000232.shtml

[53] P. M. Martin, D. W. Matson, W. D. Bennett, Y. Lin, and D. J. Hammerstrom, "Laminated plastic microfluidic components for biological and chemical systems," *Journal of Vacuum Science & Technology A*, vol. 17, no. 4, pp. 2264–2269, 1999.

[54] R. Irawan, T. S. Chuan, and F. C. Yaw, "Integration of a fluorescence detection system and a laminate-based disposable microfluidic chip," *Microwave and optical technology letters*, vol. 45, no. 5, pp. 456–460, 2005.

[55] P. K. Yuen and V. N. Goral, "Low-cost rapid prototyping of flexible microfluidic devices using a desktop digital craft cutter," *Lab on a Chip*, vol. 10, no. 3, pp. 384–387, 2010.

[56] D. Taylor, D. Dyer, V. Lew, and M. Khine, "Shrink film patterning by craft cutter: complete plastic chips with high resolution/high-aspect ratio channel," *Lab on a Chip*, vol. 10, no. 18, pp. 2472–2475, 2010.

[57] C. C. Dupont-Gillain, Y. Adriaensen, S. Derclaye, and P. Rouxhet, "Plasma-oxidized polystyrene: wetting properties and surface reconstruction," *Langmuir*, vol. 16, no. 21, pp. 8194–8200, 2000.

[58] J. Li, K. Oh, and H. Yu, "Surface rearrangements of oxygen plasma treated polystyrene: Surface dynamics and humidity effect," *Chinese journal of polymer science*, vol. 23, no. 02, pp. 187–196, 2005.

[59] A. Larsson and H. Dérand, "Stability of polycarbonate and polystyrene surfaces after hydrophilization with high intensity oxygen rf plasma," *Journal of colloid and interface science*, vol. 246, no. 1, pp. 214–221, 2002.

[60] E. C. Jameson, *Electrical discharge machining*. Society of Manufacturing Engineers, 2001.

[61] R. Kumar and S. Singh, "Current research trends in wire electrical discharge machining: An overview," *International Journal on Emerging Technologies*, vol. 3, no. 1, pp. 33–40, 2012.

[62] A. Puri and B. Bhattacharyya, "An analysis and optimisation of the geometrical inaccuracy due to wire lag phenomenon in wedm," *International journal of Machine tools and manufacture*, vol. 43, no. 2, pp. 151–159, 2003.

[63] S. S. Mahapatra and A. Patnaik, "Parametric optimization of wire electrical discharge machining (wedm) process using taguchi method," *Journal of the Brazilian Society of Mechanical Sciences and Engineering*, vol. 28, no. 4, pp. 422–429, 2006.

[64] L. Philippe, C. Heiss, and J. Michler, "Electroplating of stainless steel," *Chemistry of Materials*, vol. 20, no. 10, pp. 3377–3384, 2008.

[65] J. W. Dini, *Electrodeposition: the materials science of coatings and substrates*. Noyes Publications, 1993.

[66] S. Strahl, A. Husar, and J. Riera, "Experimental study of hydrogen purge effects on performance and efficiency of an open-cathode proton exchange membrane fuel cell system," *Journal of Power Sources*, vol. 248, pp. 474–482, 2014.

[67] J. Yang, F. Cheng, J. Liang, and J. Chen, "Hydrogen generation by hydrolysis of ammonia borane with a nanoporous cobalt–tungsten–boron–phosphorus catalyst supported on ni foam," *International journal of hydrogen energy*, vol. 36, no. 2, pp. 1411–1417, 2011.

[68] A. Brockman, Y. Zheng, and J. Gore, "A study of catalytic hydrolysis of concentrated ammonia borane solutions," *International Journal of Hydrogen Energy*, vol. 35, no. 14, pp. 7350–7356, 2010.